Physiological Reports

Open Access

Physiological Reports ISSN 2051-817X

ORIGINAL RESEARCH

Differences in ionic currents between canine myocardial and Purkinje cells

Mario Vassalle & Leonardo Bocchi

Department of Physiology and Pharmacology, State University of New York, Downstate Medical Center, 450 Clarkson Avenue, Brooklyn, NY, 11203

Keywords
Cardiac electrophysiology, ionic currents, single ventricular myocardial and cardiac Purkinje cells, whole cell patch clamp method.

Correspondence
Mario Vassalle, Department of Physiology and Pharmacology, MSC 31, SUNY Downstate Medical Center, 450 Clarkson Avenue, Brooklyn, NY 11203-2098.
Tel: (718) 270-1158
Fax: 718-270-3103
E-mail: mario.vassalle@downstate.edu

Present Address
Leonardo Bocchi, Dipartimento di Bioscienze, Università di Parma, Viale Usberti 11/A, 43124, Parma, Italy

Funding Information
This work was supported in part by a grant from the National Institutes of Health (HL56092).

Received: 5 April 2013; Revised: 20 June 2013; Accepted: 23 June 2013

doi: 10.1002/phy2.36

Physiol Rep, 1 (3), 2013, e00036, doi: 10.1002/phy2.36

Abstract

An electrophysiological analysis of canine single ventricular myocardial (VM) and Purkinje (P) cells was carried out by means of whole cell voltage clamp method. The following results in VM versus P cells were obtained. I_{Na3} was present, had a threshold negative to the fast activating–inactivating I_{Na1}, its slow inactivation was cut off by I_{Na1}, and contributed to Na^+ influx at I_{Na1} threshold. I_{Na1} was smaller and had a less negative threshold. There was no comparable slowly inactivating I_{Na2}, accounting for the shorter action potential. Slope conductance at resting potential was about double and decreased to a minimum value at the larger and less negative I_{K1} peak. The negative slope region of I-V relation was smaller during fast ramps and larger during slow ramps than in P cells, occurred in the voltage range of I_{K1} block by Mg^{2+}, was not affected by a lower V_h and TTX and was eliminated by Ba^{2+}, in contrast to P cells. I_{Ca} was larger, peaked at positive potentials and was eliminated by Ni^{2+}. I_{to} was much smaller, began at more positive values, was abolished by less negative V_h and by 4-aminopyridine, included a sustained current that 4-aminopyridine decreased but did not eliminate. Steeper ramps increased I_{K1} peak as well as the fall in outward current during repolarization, consistent with a time-dependent block and unblock of I_{K1} by polyamines. During repolarization, the positive slope region was consistently present and was similar in amplitude to I_{K1} peak, whereas it was small or altogether missing in P cells. The total outward current at positive potentials comprised a larger I_{K1} component whereas it included a larger I_{to} and sustained current in P cells. These and other results provide a better understanding of the mechanisms underlying the action potential of VM and P cells under normal and some abnormal (arrhythmias) conditions.

Introduction

The different functions of Purkinje (P) and ventricular myocardial (VM) cells are associated with several electrophysiological and mechanical differences (e.g., see Lin and Vassalle 1978; Cordeiro et al. 1998). Thus, the action potential (AP) of canine P fibers is longer (+71%, Lin and Vassalle 1978), their plateau is more negative (e.g., Baláti et al. 1998) and their twitch is shorter (−40%) and smaller (−79%) (Lin and Vassalle 1978) than in ventricular myocardial fibers.

The longer AP of P cells appears related to a greater Na^+ influx during the plateau through the slowly inactivating sodium current I_{Na2} (Vassalle et al. 2007; Bocchi and Vassalle 2008). Indeed, the Purkinje fiber AP is markedly shortened by tetrodotoxin (TTX; Coraboeuf et al. 1979; Vassalle and Bhattacharyya 1980; Bhattacharyya and Vassalle 1982; Iacono and Vassalle 1990; Baláti et al. 1998) and by local anesthetics (Vassalle and Bhattacharyya 1980; Bhattacharyya and Vassalle 1981), whereas is prolonged by high $[Na^+]_o$ and the Na^+-channel agonist verat-

ridine (Iacono and Vassalle 1990). In contrast, AP duration of ventricular myocytes is very little affected by TTX (Coraboeuf et al. 1979; Bhattacharyya and Vassalle 1982; Iacono and Vassalle 1990; Baláti et al. 1998), by local anesthetics (Vassalle and Bhattacharyya 1980), by veratridine and high $[Na^+]_o$ (Iacono and Vassalle 1990).

These findings suggest that sodium influx during the action potential may be greater in Purkinje fibers because it also includes I_{Na2}, which slowly inactivates at plateau potentials (Vassalle et al. 2007; Bocchi and Vassalle 2008). In addition, in P cells the slowly inactivating sodium current I_{Na3} is activated at potential negative to that of I_{Na1} threshold (Rota and Vassalle 2003). Whether I_{Na2} and I_{Na3} are also present in VM cells or whether Na^+ currents have identical features in P and VM cells have not been determined.

Furthermore, it is not known whether there are differences in negative slope (NS) and positive slope (PS) regions of the I-V relation between the two tissues. In P cells, I_{Na3} and I_{Na2} are involved in the NS region (Rota and Vassalle 2003), but the role of the block and unblock of inward rectifying I_{K1} channels (Ishihara 1997; Ishihara and Ehara 1998) in the NS and PS regions, respectively, is undefined. Furthermore, whether the mechanisms underlying NS and PS region are similar or differ in P and VM cells is unknown.

There are differences in electrophysiological features of other currents as rabbit P cells express smaller I_{K1}, a larger transient outward current I_{to} than VM cells (Cordeiro et al. 1998) and a greater I_{to} sensitivity to TEA (Han et al. 2000). Whether voltage-and time-dependent features of I_{K1}, I_{to}, sustained current, and I_{Ca} differ in P and VM cells have not been determined.

The general aim of the present experiments was to investigate several ionic currents by means of a whole cell patch clamp method in canine P and VM cells isolated with the same technique to determine their features (e.g., presence or absence, threshold potential, magnitude, time- and voltage-dependent characteristics).

The specific aims included the determination of differences in the following features in P and VM cells: (1) I_{K1} inward rectification and its characteristics; (2) slope conductance over the voltage range of the action potential; (3) presence of I_{Na3} and I_{Na2} and their characteristics; (4) I_{Na1} amplitude; (5) threshold potential for different Na^+ currents and their voltage- and time-dependent inactivation; (6) contribution of I_{Na3} to peak I_{Na1}; (7) presence and magnitude of NS and PS regions and their underlying mechanisms; (8) I_{to} peak and sustained outward current; (9) magnitude and voltage range of the inward component related to I_{Ca}; and (10) identification of the various currents by different means including different V_h, different ramps slopes, and channel blockers.

It was found that the differences in ionic currents between P and VM cells are numerous and substantial and provide insights in the different mechanisms that shape the action potentials, in their modification by some physiological and pharmacological factors and in the mechanisms of induction of some ventricular arrhythmias.

Material and Methods

Institutional and national guide for the care and use of laboratory animals was followed. The protocols for the experiments were reviewed and approved by the local Animal Care and Use Committee.

The details of the methods have been published (Rota and Vassalle 2003; Vassalle et al. 2007; Bocchi and Vassalle 2008). In brief outline, adult dogs (beagle, $n = 25$) of either sex were euthanized by intravenous injection of sodium pentobarbital (60 mg kg^{-1}). Once the respiration had stopped, the hearts were removed and rinsed in physiological saline solution. Purkinje fiber bundles and thin papillary muscles or trabeculae (diameter ≤ 1 mm) were cut from both ventricles and were driven at 60/min for 30 min while being superfused in a tissue bath at 37°C.

The composition of physiological saline solution in mmol L^{-1} was NaCl 140, KCl 5.4, $CaCl_2$ 1.8, $MgCl_2$ 1, HEPES 5.0, and glucose 5.5. The solution was gassed with 100% O_2 and adjusted to pH 7.4 with NaOH. The P and VM fibers were then rinsed with Ca-free solution with added 25 mmol L^{-1} taurine, 5 mmol L^{-1} beta-hydroxybutyric acid and 5 mmol L^{-1} Na pyruvate for 5 min in the same tissue bath and washed in a test tube three times with the same Ca-free solution. Ca-free solution contained in mmol L^{-1}: NaCl 140, KCl 5.4, KH_2PO_4 1.2, $MgCl_2$ 1.5, HEPES 5.0, and glucose 5.5 (pH adjusted to 7.2 with NaOH).

P and VM tissues were separately digested at 37.5°C in Ca-free physiological saline solution to which collagenase (1 mg/mL, type VIII, Sigma, St. Louis, MO), elastase (0.6 mg/mL, type II-A, Sigma), and essentially fat-free bovine serum albumin (2 mg/mL) had been added ("enzyme solution"). The cells were separated from the digested fibers by agitation by means of a mechanical "triturator" (Datyner et al. 1985). The cells were suspended in Kraftbrühe (KB) solution and samples of the cell suspension were perfused with physiological saline solution at 37°C in a chamber located on the stage of an inverted microscope (Nikon Diaphot, Nikon, Tokyo, Japan).

Whole cell patch clamp technique was employed using an Axopatch 1D amplifier. The pipettes were filled with the following solution (in mmol L^{-1}): K-aspartate 100, KCl 30, $MgCl_2$ 2.0, EGTA 11.0, Na-HEPES 10.0, Na_2-ATP 2.0, NaGTP 0.1, $CaCl_2$ 5.0 (pH 7.2) (resistance of filled pipettes 2–4 MΩ). The free Ca^{2+} in the pipette solution was 110 nmol L^{-1} as calculated using a computer

program (WinMAXC 2.40; http://stanford.edu/cpatton/maxc.html). The electrical signals were digitized at 333 kHz 12-bit resolution using A/D converter (Digidata 1200, Axon Instruments, Foster City, CA) and recorded using Clampex software (pCLAMP 8.0, Axon Instruments) and low-pass filtering at 2 kHz.

We elected to study ionic current profiles under physiological conditions (intact intracellular and extracellular ionic concentration and absence of channel blockers). Although this approach does not allow to fully isolate single currents, it preserves ionic balances and electrochemical gradients during the acquisition. Therefore, the currents in P and VM cells were studied in the absence of any channel blocker (such as Ba^{2+}, Ni^{2+}, tetrodotoxin, 4-Aminopyridine, etc.) to compare and contrast the currents under physiological conditions and to avoid the multiple effects of channel blockers on currents and ionic gradients. Later on, we identified the current under study and their role on different parameters in different ways, including different V_h, different ramps slopes, and channel blockers.

Successive command steps of the same protocol were applied at intervals of at least 5 sec and different protocols were separated by intervals of 3–5 min to allow the effects of each procedure to fully subside.

The data were analyzed by means pCLAMP program (Axon Instruments Inc.). Steps from different holding potentials (V_h) were applied to activate voltage- and time-dependent currents and depolarizing and repolarizing ramps with different slopes were used to study the currents under different conditions. On step depolarization from V_h −80 mV, I_{Na1} was often cut off at −10 nA by the saturation of the amplifier. As no differences were detected in the results obtained from male and female dog cells, the results were pooled together.

The amplitude of the slowly decaying component of I_{Na2} was measured as the difference between the current at the beginning and the end of the step. The beginning was taken as the value at the intersection between the rapidly inactivating I_{Na1} and the backward extrapolation of I_{Na2}, also checked by fitting the slowly inactivating I_{Na2} with a double exponential function.

Unless otherwise specified, the current traces were fitted with two term standard exponential function using the Chebyshev technique with Clampfit software according to equation (1):

$$I(t) = A_1 exp(-t/\tau_s) + A_2 exp(-t/\tau_f) + C \qquad (1)$$

where A_1 and A_2 are the amplitudes, and τs and τf are the time constants and C is the offset constant.

Data were analyzed by mean of the Clampfit (pCLAMP 10.2) and Microsoft Excel programs. The results of tests carried out for each procedure are shown in the tables as means ± SEM (standard error of the mean) together with the number (n) of cells studied. Student's paired t test between two terms of comparison and one-way ANOVA (analyses of variance) between a data group were applied and a $P < 0.05$ was considered significant and was marked by an asterisk (*) in the tables and in text.

Results

I_{Na3} and its relation to I_{Na1}

In P cells, I_{Na3} appears at a potential (−57.8 mV) which is negative to I_{Na1} threshold (−52 mV) (Rota and Vassalle 2003). I_{Na1} suppresses the slow inactivation of I_{Na3}, as at its threshold I_{Na1} is not followed by time-dependent current (Rota and Vassalle 2003; Vassalle et al. 2007; Bocchi and Vassalle 2008). Whether I_{Na3} also is present in VM cells or whether its slow inactivation is suppressed by I_{Na1} is not known.

In Figure 1A, in a VM cell during the step from V_h −80 mV to −50 mV, an inward current appeared that decayed bi-exponentially. In Figure 1B, the step to −40 mV elicited I_{Na1} (partially shown), which (as in P cells) was not followed by a slowly inactivating component. In Figure 1 inset 1, the shaded area emphasizes the fact that I_{Na3} slow inactivation was present at −50 mV and absent at −40 mV.

The absence of I_{Na3} during the step at I_{Na1} threshold potential could be due to either the suppression of I_{Na3} slow inactivation by I_{Na1} (as in P cells) or to the less negative voltage. To clarify this point, a two-step protocol was applied, as a suitable conditioning step may reduce I_{Na1} channel availability just enough to shift its threshold to a less negative value. In Figure 1C, the conditioning step to −50 mV induced I_{Na3} and the test step to −40 mV failed to activate I_{Na1} and induced a smaller I_{Na3}. The finding suggests that in Figure 1B I_{Na3} inactivation was not present because it was suppressed by I_{Na1} and not because it could not occur at −40 mV.

In Figure 1D, the −30 mV test step initiated an inward transient (−3037 pA) which was followed by a small shallow tail (−93 pA), suggesting the induction of I_{Na2} with a small slow inactivation component.

In n = 10, with the two steps protocol in VM cells during the step from −80 mV to −50 mV I_{Na3} amplitude was −143.2 ± 54.9 pA and during the test step to −40 mV it was −72.4 ± 9.9 pA (not significantly different). During the test step to −30 mV, the inward transient was −3045 ± 576 pA and was followed by a decaying tail of 63.7 ± 14.8 pA. Therefore, in VM cells I_{Na3} was present during the −40 mV test step in the absence of I_{Na1}. During the −30 mV test step, I_{Na2} was followed by a small and quickly inactivating component

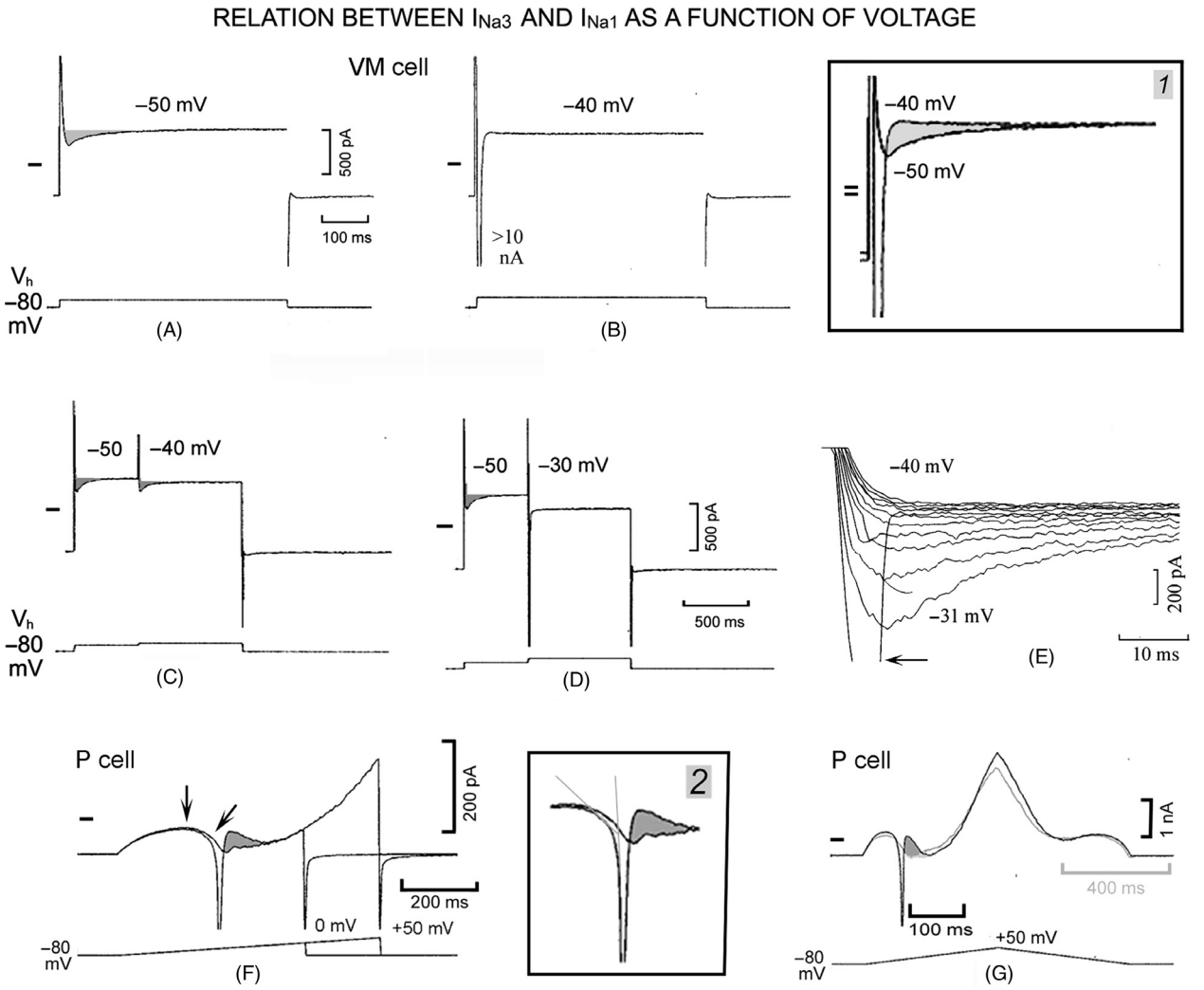

Figure 1. I_{Na3} and its relation to I_{Na1}. In a VM cell, a depolarizing step from V_h −80 mV to −50 mV (lower trace in A) and to −40 mV (B) elicited the currents shown in the upper traces. The current traces have been superimposed in inset 1 and the shaded area emphasizes the suppression of the slow inactivation of I_{Na3} by I_{Na1}. In C, a conditioning step was applied to −50 mV and a test step to −40 mV and in D to −50 and −30 mV, respectively. In E, depolarizing steps were applied from V_h −80 to −40 mV and increased by 1 mV to −30 mV: the horizontal arrow points to inactivating I_{Na1}. In F, in a P cell, ramps with the same slope and different duration were applied. Downward vertical arrow points to I_{K1} peak and downward oblique arrow to the negative slope region. In inset 2, part of the F traces are shown at greater gain. Dashed lines emphasize the different slopes of inward currents prior to and at beginning of I_{Na1}. In F and G, the shaded areas show that at the end of I_{Na1} inactivation the magnitude of the outward current approached that of I_{K1} peak. The short dash in each panel indicates zero current in this and subsequent figures. In G, ramps with different slopes (260 mV sec^{-1}, gray trace; 520 mV sec^{-1}, black trace) were applied.

(see below). Similarly, in P cells (n = 10) I_{Na3} could be activated at the I_{Na1} threshold if the activation of I_{Na1} was prevented by the conditioning step. One difference with the VM cells was that in P cells the slowly inactivating I_{Na2} was much larger (+673.1%*; see below).

I_{Na3} was studied in VM and P cells by applying single steps (Fig. 1A) from V_h −80 mV (Table 1). With respect to P cells, in VM cells during depolarizing steps I_{Na3} was consistently present, had a less negative threshold (*), and similar amplitude as well as time constants of inactivation.

The finding that the −50 mV conditioning step prevented the appearance of I_{Na1} but not of I_{Na3} during the −40 mV test step suggests that I_{Na3} might be less sensitive to voltage-dependent inactivation than I_{Na1}. This was tested by applying depolarizing steps from gradually less negative V_h. As shown in Table 1, in P and VM cells with gradually less negative V_h, the amplitude of I_{Na3} decreased very little until V_h was −40 mV and the threshold remained less negative (*) in VM cells. At all V_h, in both P and VM cells the inactivation of I_{Na3} was slow in the

Table 1. I_{Na3} in P and VM cells and its changes with lower V_h.

V_h (mV)	Param	VM cells	P cells
−80	Th (mV)	−46.7 ± 1.1	−53.3 ± 1.9*
	I_{Na3} (pA)	−168 ± 52 (18/18)	−217 ± 102 (13/18)
	τ_f (msec)	15.3 ± 2.9	10.5 ± 2.8
	τ_s (msec)	82.7 ± 11.9	55.9 ± 12.9
−70	Th (mV)	−43.3 ± 1.3	−52.5 ± 1.8*
	I_{Na3} (pA)	−189 ± 66 (15/16)	−190 ± 63 (11/16)
−60	Th (mV)	−38.5 ± 1.0	−46.6 ± 1.2*
	I_{Na3} (pA)	−120 ± 29 (12/15)	−235 ± 71 (14/15
−50	Th (mV)	−33.6 ± 1.5	−35.6 ± 2.0
	I_{Na3} (pA)	−179 ± 76 (11/16)	−155 ± 42 (14/16)
−40	Th (mV)	−21.0 ± 1.0	−27.1 ± 1.8*
	I_{Na3} (pA)	−29.9 ± 18.3 (3/10)	−84 ± 35 (6/9)

V_h (mV), holding potential in mV; Param, parameters measured; VM cells, data from ventricular myocardial cells; P cells, data from Purkinje cells; Th (mV), threshold potential in mV of I_{Na3}; I_{Na3} (pA), amplitude in pA of I_{Na3} measured as the difference between its peak and the end of the step; τ_f (msec) and τ_s (msec), fast and slow time constants, respectively, of I_{Na3} inactivation; Numbers in parenthesis (e.g., 18/18), number of cells in which I_{Na3} was present over the total number of cells studied; *statistically significant difference between P and VM cells data.

absence of I_{Na1}. Even with V_h −40 mV, I_{Na3} inactivated with τ_f 13.1 ± 7.5 msec and τ_s 41.3 ± 18.5 msec in VM cells and with τ_f 7.5 ± 1.4 msec and τ_s 82.1 ± 22.6 msec in P cells.

I_{Na3} voltage-dependent increase and sudden suppression of its slow inactivation by I_{Na1}

Gradually increasing depolarizing steps might lead to a progressive increase in I_{Na3}. In Figure 1E, in a VM cell with depolarizing steps increasing by 1 mV between the I_{Na3} and I_{Na1} thresholds, I_{Na3} magnitude increased progressively and inactivated relatively more quickly up to −29 mV. At −30 mV (I_{Na1} threshold), the inactivation of I_{Na1} (arrow) suppressed I_{Na3} slow decay. Similar results with steps increasing at intervals of 1 mV were obtained in VM cells (n = 4) and in P cells (n = 16).

The above results suggest that during depolarizing ramps I_{Na3} might precede I_{Na1}, as the continuous decline in voltage would initiate and increase I_{Na3} at potentials negative to the I_{Na1} threshold. Furthermore, the current at the end of I_{Na1} inactivation would be expected to be more outward than in its absence due to the suppression of I_{Na3} slow inactivation. In some cells, applying ramps of different duration with a borderline slope (150 mV sec^{-1}) for I_{Na1} activation led to a nonuniform induction of I_{Na1}, so that the events in the presence and absence of I_{Na1} could be compared in the same cell as shown in Figure 1F.

In a P cell, during the ramps, the outward current gradually increased before peaking (I_{K1} peak, vertical arrow). The slope of the ramps being borderline for I_{Na1} activation, during the shorter ramp, I_{K1} peak was followed by a negative slope (NS) region (oblique arrow). No I_{Na1} was present and the current during the NS region (I_{NS}) was followed by a reincreasing outward current. During the longer ramp, I_{NS} more quickly turned inward and its steeper slope merged into that of the activating I_{Na1}, as emphasized by the gray lines in Figure 1 inset 2.

In Figure 1F and inset 2, the shaded area shows that the current at the end of I_{Na1} inactivation was more outward than in the I_{Na1} absence, as expected from the suppression of the slow inactivation of I_{Na3} by I_{Na1}. The inactivation of I_{Na1} was still followed by NS region with smaller amplitude and less steep slope, consistent with the slow inactivation of I_{Na2} (see below). The patterns illustrated in Figure 1F were present in n = 3, the consistent presence of I_{Na1} with its inactivation approaching I_{K1} peak in n = 4 and the absence of I_{Na1} with the consistent presence of I_{NS} in n = 19.

In another approach, ramps with different slopes (Fig. 1G) were applied, as in several instances in P cells no I_{Na1} was initiated during slower ramps. In Figure 1G, the 260 mV sec^{-1} ramp (lighter trace) did not activate I_{Na1}, whereas the superimposed 520 mV sec^{-1} ramp (darker trace) did. During the slower ramp, I_{K1} peak was followed by I_{NS} but not by I_{Na1}. Instead, with the steeper ramp, the end of I_{Na1} inactivation approached the I_{K1} peak and was followed by I_{NS}.

The asymmetry between slower activation and faster inactivation of the overall Na^+ current (Fig. 1 F and G) was a consistent finding that might be expected from I_{Na3} preceding I_{Na1} and its slow inactivation being cut off by it.

In VM cells, I_{Na1} was less frequently absent with slower ramps. With 260 mV sec^{-1} ramps, I_{Na1} was absent in 9/17 P cells and in 3/17 VM cells whereas with the 520 mV sec^{-1} ramp, I_{Na1} was absent only in 3/17 P cells and in none of 17 VM cells (the NS region being present with or without I_{Na1}).

Therefore, in VM cells I_{Na3}: (1) was present with a similar magnitude and rate constants of inactivation; (2) had a threshold less negative than in P cells and negative to that of I_{Na1}; (3) increased progressively at potentials between its threshold and that of I_{Na1}; (4) its slow inactivation was consistently eliminated by I_{Na1}; (5) could appear and inactivate slowly at voltages less negative than I_{Na1} threshold if I_{Na1} activation was prevented by a conditioning step; (6) contributed to the beginning of I_{NS} during depolarizing ramps, and (7) was less sensitive than I_{Na1} to voltage- and time-dependent inactivation.

Currents during larger depolarizing steps in Purkinje and myocardial cells

Ionic currents in P and VM cells were investigated also by applying 500 msec depolarizing steps from V_h −80 mV to +40 mV in increments of 10 mV (Fig. 2, protocol in c).

In Figure 2, in the P cell (A) the range of inward and outward currents was larger than in the VM cell (Fig. 2B). In P cell, I_{Na1} was truncated by the saturation of the amplifier at −10,000 pA whereas in VM cell the largest I_{Na1} was −8428 pA. In the P cell (Fig. 2c), the −50 mV step initiated I_{Na1} whose inactivation was followed by a steady current that overlapped the current trace at −60 mV (where no I_{Na1} was present; see also Vassalle et al. 2007; Bocchi and Vassalle 2008), thus suggesting no loss of voltage control. The slowly inactivating I_{Na2} appeared at −40 mV and reached its largest value during −20 mV step (shaded area in Fig. 2c). Typically, I_{Na2} was still decreasing by the end of the 500 msec step (Vassalle et al. 2007; Bocchi and Vassalle 2008).

In the VM cell, the threshold for I_{Na1} activation was less negative (−40 mV, Fig. 2d) than in the P cell (−50 mV). During the depolarizing −20 mV step, the inactivation of I_{Na1} was not followed by a decaying I_{Na2}, in contrast to the P cell. The comparison of Figure 2a and b indicates that in VM cell the large and slowly decaying I_{Na2} was absent at other potentials as well. The

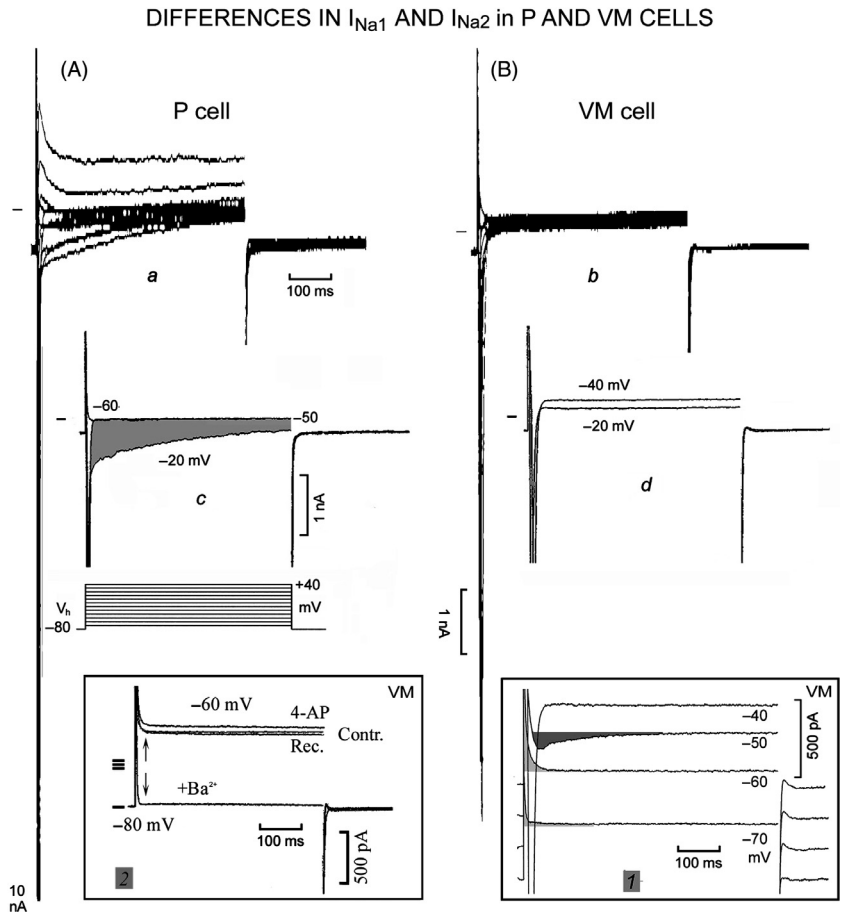

Figure 2. Larger range of inward and outward currents in P than in VM cells. The protocol is shown at the bottom of c. In the P cell, the currents flowing during the steps from V_h −80 to −60, −50, and −20 mV are shown in c, where the shaded area emphasizes the slow decay of I_{Na2}. In the VM cell, the currents recorded with steps from V_h −80 to −40 and −20 mV are shown in d. In inset 1, the current traces were displaced by 200 pA for a better visualization. The light-shaded areas emphasize the time-dependent component of I_{K1} and the dark-shaded area I_{Na3}. In inset 2, the current traces during the −60 mV step are shown in control (Contr.) in the presence of 4-aminopyridine (4-AP), of 4-AP plus Ba^{2+} (+Ba^{2+}), and during recovery (Rec.). The upward arrow indicates the initial decline in the outward current to a steady value and the downward arrow its suppression by Ba^{2+}.

sustained current at the end of −50 mV step (measured as the difference from the holding current I_h) was larger in the VM cell than in the P cell. In the VM cell, the sustained current at −40 mV (I_{Na1} threshold) was similar to that at −50 mV (not shown). In both cells, the sustained current at −20 mV was less outward than at −50 mV (P cell) and at −40 mV (VM cell), as expected from the onset of I_{NS}. With more positive steps, the outward currents were far larger in P cell than in VM cell (cf. Fig. 2a and b).

In Table 2, with V_h −80 mV, in VM cells I_{Na1} threshold was less negative in P cells (*), I_{Na1} was smaller (*) in VM cells, as it was truncated in all P cells, but only in 13/18 VM cells. In both VM and P cells, I_{Na1} inactivated exponentially with τ ~1.5 msec. In VM cells, I_{Na1} was smaller (*) than in P cells also with V_h −70 mV when I_{Na1} was less often truncated.

In Table 3, at −20 mV in VM cells an inactivating I_{Na2} tail was present in 6/18 cells, was small and decayed quickly. In contrast, in P cells the slowly inactivating I_{Na2} was much larger (*) and inactivated more slowly (*). With gradually less negative V_h, I_{Na1} (Table 2) and I_{Na2} (Table 3) gradually decreased.

The slope conductance was measured by superimposing small hyperpolarizing pulses on the parent steps in VM cells (n = 9). At the I_{Na1} threshold, after the I_{Na1} inactivation, the slope conductance was minimal and did not vary with time, as shown in P cells by Bocchi and Vassalle (2008). This finding also is consistent with no loss of voltage control.

Time-dependent decay of I_{K1} on depolarization in Purkinje and myocardial cells

In Figure 2, in the same VM cell, the currents during the −70, −60, −50, and −40 mV steps are shown in inset 1. At the beginning of the −70 and −60 mV steps, the outward current quickly declined (light-shaded areas) to a steady value. At −50 mV, I_{Na3} appeared and declined slowly (dark-shaded area), and at −40 mV I_{Na1} quickly activated and inactivated to a steady value.

One possible explanation for the initial decline of the outward current at −60 and −70 mV might be a noninstantaneous block of I_{K1} by polyamines during the depolarizing steps (Ishihara 1997; Ishihara and Ehara 1998), a block which is eliminated by Ba^{2+} (Ishihara and Ehara 1998). In Figure 2 inset 2, the traces during the step to −60 mV were recorded in control (Contr.), in the presence of 4-aminopyridine (4-AP), of Ba^{2+} ($+Ba^{2+}$), and during recovery (Rec.). The upward arrow indicates the initial decline in the outward current to a steady value, a decline that was little affected by 4-AP. Instead, Ba^{2+} suppressed both the initial decay and the steady current during the step (downward arrow).

In Table 4, with V_h −80 mV, at the voltages indicated in VM cells the outward current decreased more (*) in VM cells than in P cells. The time constant of the exponential decline was similar (~6 msec).

If the decline of the current during the step is indeed due to a time-dependent block of I_{K1} on depolarization, then

Table 2. I_{Na1} in P and VM cells and its changes with lower V_h.

V_h (mV)	Param	VM cells	P cells
−80	Th (mV)	−36.7 ± 1.1	−48.3 ± 1.5*
	I_{Na1} (pA)	−8857 ± 461 (18/18)	−10, 000 ± 0.0* (18/18)
	τ (msec)	1.3 ± 0.2	1.6 ± 0.2
−70	Th (mV)	−33.7 ± 1.2	−43.1 ± 1.8*
	I_{Na1} (pA)	−8551 ± 445 (16/16)	−9622 ± 263.0* (16/16)
	τ (msec)	1.5 ± 0.2	1.6 ± 0.2
−60	Th (mV)	−30.7 ± 1.5	−34.7 ± 1.7
	I_{Na1} (pA)	−6167 ± 959 (15/15)	−7984 ± 844 (15/15)
	τ (msec)	1.4 ± 0.2	1.6 ± 0.2
−50	Th (mV)	−23.3 ± 1.4	−26.0 ± 1.3
	I_{Na1} (pA)	−2153 ± 618 (11/16)	−3404 ± 820 (14/16)
	τ (msec)	2.4 ± 0.7	1.6 ± 0.1
−40	Th (mV)	−13.3 ± 3.3	−18.75 ± 1.3
	I_{Na1} (pA)	−58.1 ± 33 (3/10)	−642 ± 325 (5/8)
	τ (msec)	3.7 ± 0.6	2.9 ± 0.4

I_{Na1} (pA), amplitude of I_{Na1} from its beginning to its peak in pA; τ (msec), time constant of the exponential inactivation in ms of I_{Na1}; VM cells, data from ventricular myocardial cells; P cells, data from Purkinje cells; Th (mV), threshold potential in mV of I_{Na1}; Numbers in parenthesis (e.g., 18/18), number of cells in which I_{Na1} was present over the total number of cells studied; *statistically significant difference between P and VM cells data.

Table 3. I_{Na2} in P and inward tail in VM cells and their changes with lower V_h.

V_h (mV)	Param	VM cells	P cells
−80	Peak (mV)	−20.0 ± 0.0	−21.2 ± 0.8
	I_{Na2} slow (pA)	−110.2 ± 39.3 (6/18)	−1212 ± 208* (15/18)
	τ_f (msec)	4.0 ± 1.8	8.1 ± 1.0*
	τ_s (msec)	60.8 ± 22.1	233.9 ± 24.7*
−70	Peak (mV)	−20.0 ± 0.0	−20.6 ± 0.6
	I_{Na2} slow (pA)	−66.1 ± 25.8 (9/16)	−1985 ± 263* (15/16)
−60	Peak (mV)	−20.0 ± 0.0	−22.1 ± 1.1
	I_{Na2} slow (pA)	−46.1 ± 20.0 (5/15)	−854 ± 140* (13/15)
−50	Peak (mV)	−13.3 ± 2.1	−15.3 ± 1.6
	I_{Na2} slow (pA)	−35.7 ± 18.4 (5/16)	−382 ± 195 (9/16)

Peak (mV), voltage at which the largest slowly inactivating I_{Na2} in P cells or in VM cell was measured; I_{Na2} slow (pA), amplitude of slowly inactivating I_{Na2} in pA, measured from its beginning to the end of the step; VM cells, data from ventricular myocardial cells; P cells, data from Purkinje cells; τ_f (msec) and τ_s (msec), fast and slow time constants, respectively, of I_{Na2} inactivation; Numbers in parenthesis (e.g., 6/18), number of cells in which I_{Na2} was present over the total number of cells studied; *statistically significant difference between P and VM cells data.

decreasing V_h should reduce the declining current, as increasing degrees of I_{K1} block would occur during the less negative V_h, prior to the depolarizing step. To test this point, V_h was reduced in 10 mV increment to −40 mV. As shown in Table 4, in both P and VM cells with gradually less negative V_h, the initial decay of the current became gradually smaller and less frequent, and disappeared altogether with V_h −40 mV. These findings indicate a time- and voltage-dependent block of I_{K1}, which was significantly larger in VM cells at V_h −70 and −60 mV.

Contribution of I_{Na3} to Na^+ inflow due to I_{Na1}

As I_{Na3} occurs also at the I_{Na1} threshold, at that potential I_{Na3} would be expected to precede I_{Na1} and therefore contribute to the peak Na^+ current. To verify such a possibility, the current traces at the beginning of depolarizing steps were displayed at suitably greater time base.

In Figure 3, in a P cell (A) and in a VM cell (B), at the usual time base only I_{Na1} was visible. However, when the traces were displayed at much greater time base, a slower inward component (comprised between the downward and horizontal arrows) preceded I_{Na1} both in P (Fig. 3C) and in VM cell (Fig. 3D). In Figure 3C (P cell), the trace recorded at −60 mV show the initial decay of the outward current to a steady value (time-dependent block of I_{K1}). Instead, the trace recorded at −50 mV departed from the exponential decay (vertical arrow), crossed in an inward direction the −60 mV trace (as expected from the activation of I_{Na3}). After a delay, it was followed by the fast initiation of I_{Na1} (sudden beginning of the steeper

Table 4. I_{K1} time-dependent decay during depolarizing steps from different V_h.

V_h (mV)	Param	VM cells	P cells
−80	Measured at (mV)	−58.8 ± 0.7	−59.6 ± 6.4
	I_{K1} decay (pA)	317 ± 29 (18/18)	237 ± 24* (18/18)
	τ (msec)	6.3 ± 0.9	5.9 ± 1.2
−70	Measured at (mV)	−55.6 ± 1.2	−59.3 ± 0.6*
	I_{K1} decay (pA)	226 ± 3.7 (16/16)	62.9 ± 16.5* (11/16)
−60	Measured at (mV)	−50.0 ± 0.0	−50.0 ± 0.0
	I_{K1} decay (pA)	78.4 ± 26.2 (6/15)	21.1 ± 18.2 (2/15)
−50	Measured at (mV)	−40.0 ± 0.0	−40.0 ± 0.0
	I_{K1} decay (pA)	24.1 ± 15.6 (4/16)	12.8 ± 8.8 (2/16)

Measured at (mV), voltage in mV at which the decay of I_{K1} was measured; I_{K1} decay (pA), amplitude of I_{K1} time-dependent decay at beginning of step; τ (msec), time constant of I_{K1} exponential decay; V_h (mV), holding potential in mV; VM cells, data from ventricular myocardial cells; P cells, data from Purkinje cells; Numbers in parenthesis (e.g., 18/18), number of cells in which I_{K1} decay was present over the total number of cells studied; *statistically significant difference between P and VM cells data.

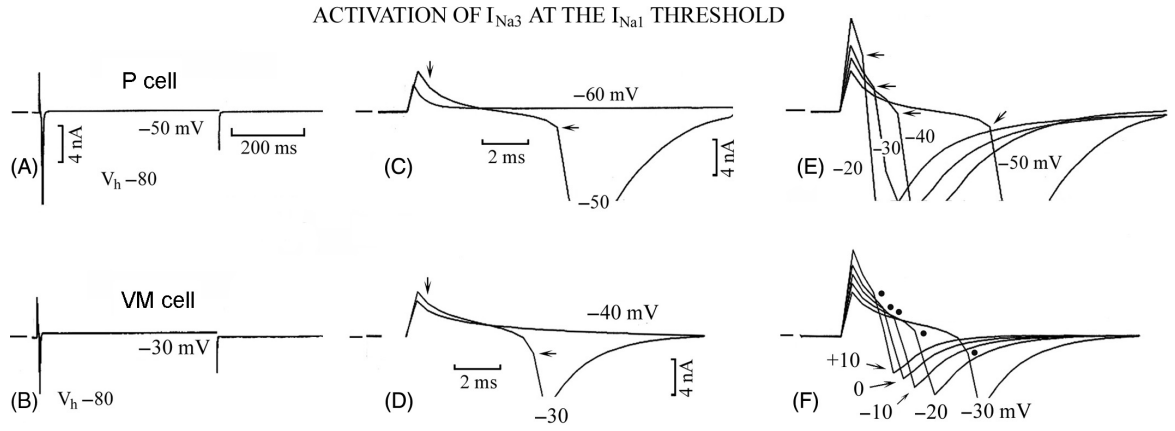

Figure 3. The activation of I_{Na3} precedes that of I_{Na1} at the latter's threshold. In A (P cell) and B (VM cell), the traces are shown at the usual time base whereas in C, D, E, and F the traces are shown at the greater time base indicated. In C and D, the downward vertical arrows point to the beginning of I_{Na3} and the leftward horizontal arrows point to the beginning of I_{Na1}. The traces recorded at the beginning of the −50, −40, −30, and −20 mV steps have been superimposed in E (P cell) and those at the beginning of the steps to −30, −20, −10, 0, and +10 mV have been superimposed in F (VM cell). The arrows in E and the dots in F indicate the beginning of I_{Na1}. The numbers next to the traces indicate the voltage of the respective steps.

slope, horizontal arrow). Similar events occurred in the VM cell (Fig. 3D).

In Figure 3E (P cell), the current traces at the beginning of −50, −40, −30, and −20 mV steps were superimposed and show the progressively earlier onset of I_{Na1} with larger depolarizing steps until no distinct I_{Na3} component was apparent. In Figure 3F, similar events occurred in the VM cell in that larger depolarizing steps elicited an earlier I_{Na1} with the eventual disappearance of I_{Na3}.

In $n = 18$, in VM cells, I_{Na3} (measured between the departure of the trace from exponential decay and the sudden onset of I_{Na1}) had a magnitude of -2677 ± 201 pA and a duration of 2.2 ± 0.3 msec; I_{Na1} (measured from the sudden increase in steepness to its peak) had a threshold of -36.6 ± 1.1 mV) and an amplitude of -8857 ± 461 pA. In P cells, I_{Na3} had a amplitude of -2330 ± 235* pA and a duration of 2.6 ± 0.8 msec; I_{Na1} had a more negative threshold (-48.3 ± 1.4* mV) and an amplitude $>-10{,}000 \pm 0.0$* pA.

Thus, I_{Na3} was a substantial fraction of the inward current flowing at the threshold for I_{Na1}. With steps to less negative values, I_{Na3} consistently decreased and I_{Na1} was activated sooner.

Differences in I-V relation of the sustained current in Purkinje and myocardial cells

To investigate the quasi-steady state I-V relations in VM and P cells, the sustained current at the end of 500 msec depolarizing steps from V_h −80 mV to +40 mV was measured as the difference from I_h. The same procedure was applied with less negative V_h to determine how the I-V relation would be affected in P versus VM cells.

In Figure 4, in A, with V_h −80 mV, in VM cells the sustained current was more outward at negative potentials and less outward at positive potential than in P cells. In both types of cells, past I_{K1} peak, the NS region was present, but in VM cells I_{NS} was larger and peaked at a less negative value (~0 mV), whereas in P cells the smaller I_{NS} peaked at ~−20 mV. The outward current began to increase at +10 mV in VM cells and at −10 mV in P cells, suggesting a different I_{to} threshold.

I_{NS} was differently affected by lower V_h in P and VM cells. With V_h −70 (Fig. 4B), overall the sustained current was much less outward in both VM and P cells, as expected from the inward rectification of I_{K1} channel at less negative V_h. However, I_{NS} was still large in VM cells whereas it was diminished in P cells, suggesting that in P cells the decrease in I_{NS} might be related to a partial inactivation of I_{Na2}.

This interpretation is supported by the findings with still lower V_h. In VM cells, the current became inward and I_{NS} persisted unaltered up to V_h −50 mV (Fig. 4B–D). Only with V_h −40 mV did I_{NS} decrease (Fig. 4E) as apparently the channel contributing to I_{NS} was partially blocked prior to the depolarizing step. Instead, in P cells I_{NS} markedly decreased with V_h −60 to disappear altogether with V_h −40 mV. In Figure 4 inset 1, the graph shows the difference between the outward current peak prior to the NS region (corresponding to I_{K1} peak) and the smallest current value of I-V relation prior to the reincrease in outward

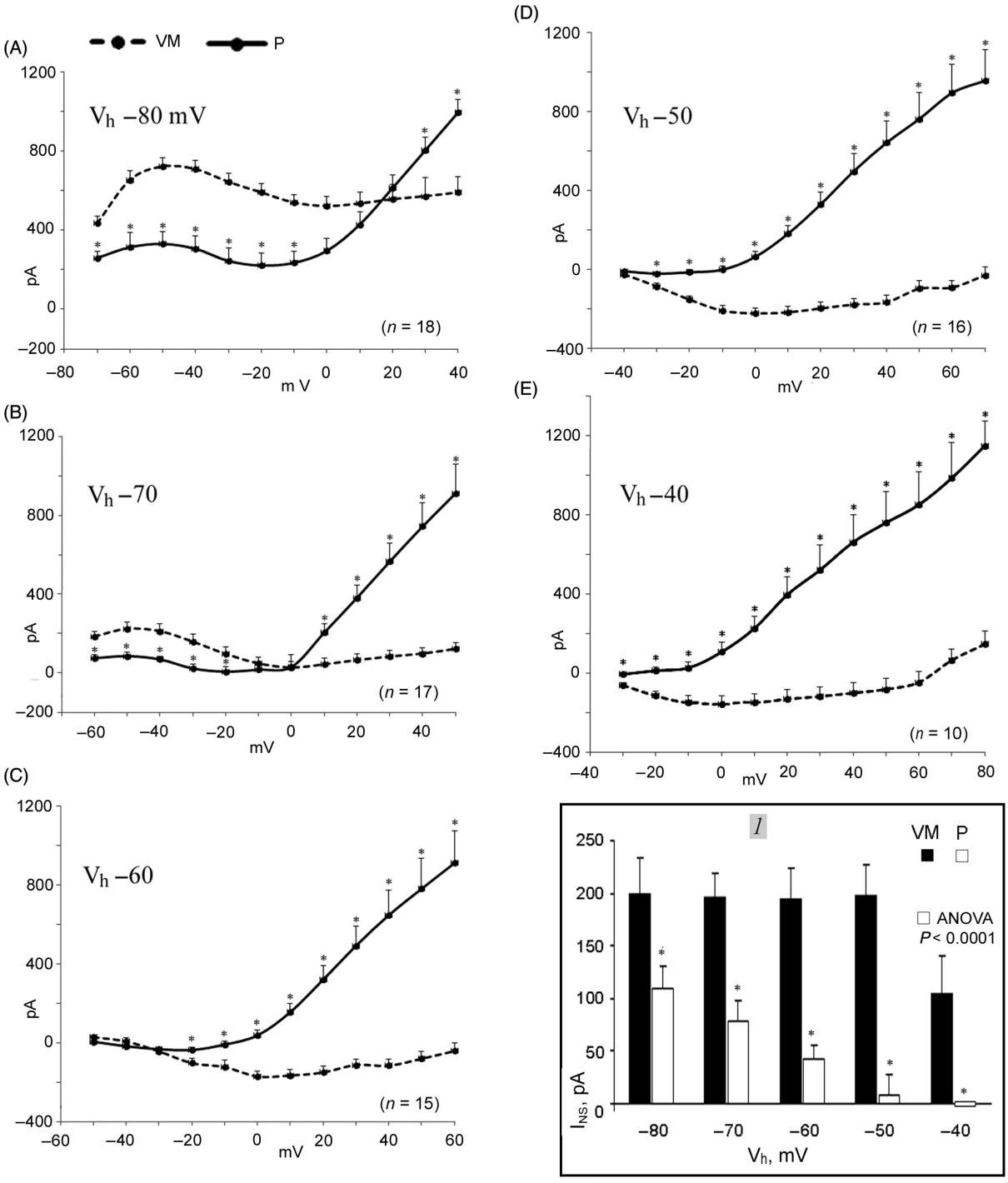

Figure 4. The I-V relation as a function of V_h in P and VM cells. The number of P and VM cells studied is indicated in parenthesis in each panel. The ordinates show the magnitude of the sustained current in pA at the end of 500 ms depolarizing steps applied from the V_h indicated in each panel to the voltage in mV indicated on the abscissae. The VM cells mean data are connected by dashed line and those of P cells by continuous line. The vertical bars indicate the standard error of the mean. In inset 1, the mean values of I_{NS} are the difference between the most outward sustained current and the subsequent least outward sustained (or the largest inward) current in pA at voltage indicated on abscissa. The asterisks (*) indicate a statistical difference between the data in VM and P cells. The difference between the values in P cells at the various V_h was statistically significant (ANOVA $P < 0.0001$).

current (a measure of I_{NS} peak). The graph shows how differently I_{NS} amplitude varied in VM and P cells as a function of V_h, the decrease of I_{NS} in P cells being statistically significant (ANOVA < 0.0001).

The increase in outward current with the larger depolarizing steps was much greater in P than in VM cells (helped in this by the inward shift of the current in VM cells), and it was little affected by less negative V_h. At each V_h, the outward current in P cells increased past ~−20 mV, as expected for I_{to}. As the protocol applied at different V_h was the same, with the gradually less negative V_h the depolarizing steps attained gradually more positive values. Hence, the sustained current with the largest depolarizations increased to similar values in spite of the decreasing V_h.

These results raise the possibility that in P cells Na^+ currents might mainly contribute to I_{NS} (with this protocol, I_{Na2}) whereas the voltage-dependent block of I_{K1} channel may predominantly determine I_{NS} in VM cells.

I_{Na2} and the I_{Ca} component in Purkinje and myocardial cells

As at plateau voltages the slowly inactivating I_{Na2} prevails in P cells and presumably I_{Ca} prevails in VM cells, the different amplitude, voltage range, voltage- and time-dependent inactivation of I_{Na2} in P cells and of the I_{Ca} component in VM cells were investigated as shown in Figure 5.

In the P cell (Fig. 5A), a step from V_h −80 to −50 mV elicited I_{Na1} which was not followed by time-dependent

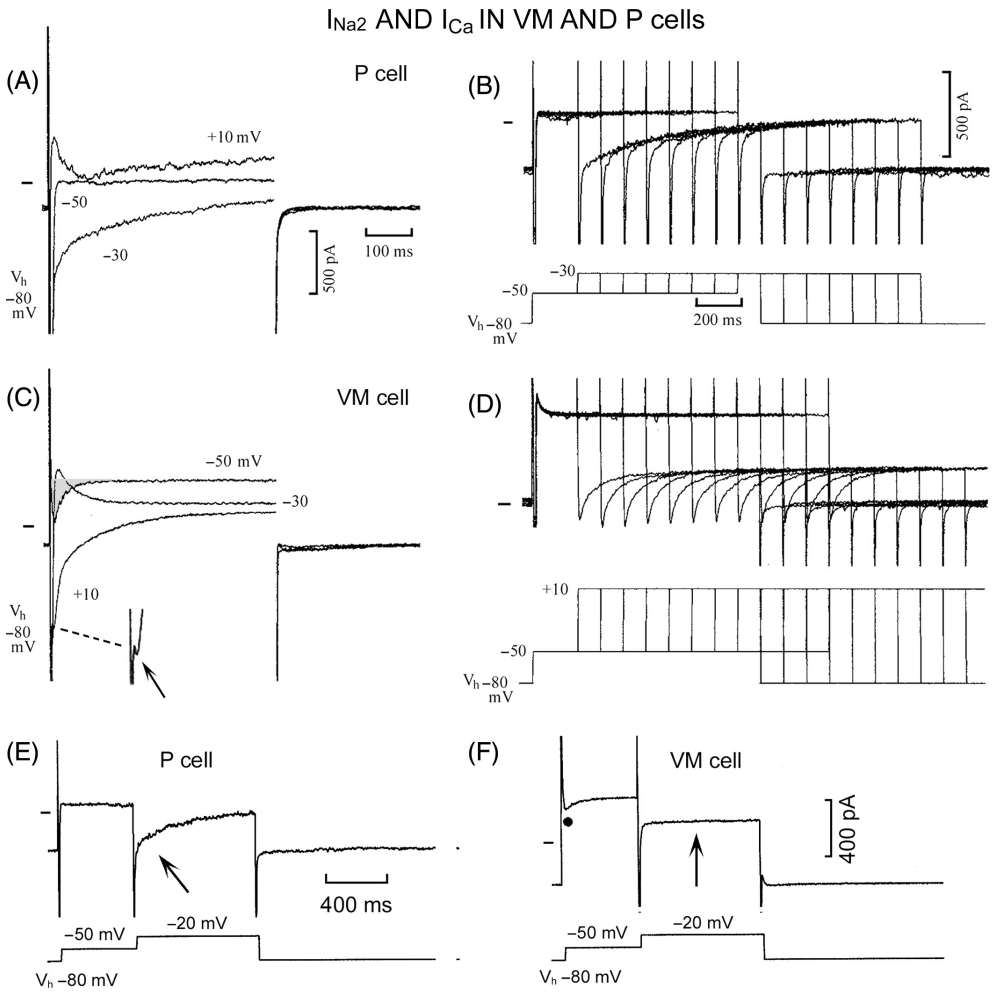

Figure 5. Different amplitude, voltage range, kinetics, and time-dependent inactivation of I_{Na2} in P cells and of I_{Ca} in VM cells. Steps were applied from V_h −80 to −50, −30 mV +10 mV in the P cell (A) and in the VM cell (C) where the shaded area emphasizes I_{Na3} and the small arrow points to the beginning of a large I_{Ca}. In the P cell (B), progressively longer conditioning steps to −50 mV were followed by test steps to −30 mV. In the VM cell (D), conditioning steps to −50 mV were followed by test steps to +10 mV. In E, the oblique upward arrow points to inactivating I_{Na2} during the test step to −20 mV in the P cell. In F, the filled circle labels I_{Na3} and the vertical upward arrow points to the absence of comparable slowly inactivating I_{Na2} at −20 mV in the VM cell.

currents, as usual. During the step to −30 mV, I_{Na1} was followed by the slowly decaying I_{Na2} (τ_s 297 msec). During the +10 mV step, a small inward component was superimposed on a small outward current. In the VM cell (Fig. 5C), the step from V_h −80 to −50 mV elicited I_{Na3} (shaded area). During the step to −30 mV, I_{Na1} was followed by a small outward component, but not by decaying I_{Na2}. During the +10 mV step, I_{Na1} was followed by a large I_{Ca} component (−1699 pA) which inactivated with a τ_s of 106 msec and whose beginning during I_{Na1} inactivation is indicated by the arrow in the magnified trace.

In the P cell (Fig. 5B), after progressively longer conditioning steps at −50 mV, the test steps to −30 mV elicited a gradually smaller inactivating I_{Na2} (with the last test step, −47%) (see Bocchi and Vassalle 2008). In the VM cell (Fig. 5D), the conditioning step was the same, but (as there was no I_{Na2} at −30 mV) test steps were applied to the voltage where I_{Ca} component was largest (+10 mV, protocol in Fig. 5D). The test step elicited an inward current, whose amplitude was not decreased by progressively longer conditioning steps (with the last test step, +3.7%). In the VM cell, I_{Ca} decayed more quickly than I_{Na2} did in the P cell. The findings point to a different voltage range, kinetics, and voltage- and time-dependent inactivation of I_{Na2} in P cells and of I_{Ca} in VM cells.

In order to separate I_{Na1} from I_{Na2}, a double step protocol was applied from V_h −80 mV to −50 and to −20 mV in a P cell (Fig. 5E) and in a VM cell (Fig. 5F). In the P cell, at −50 mV I_{Na1} was followed by a steady current, and at −20 mV I_{Na2} activated rapidly and decayed slowly (oblique arrow). In the VM cell, at −50 I_{Na3} was present as usual at that voltage (filled circle; see Fig. 1) and at −20 mV an inward transient was followed by a faint and brief tail at a potential where the slowly decaying I_{Na2} was large in the P cell.

With V_h −80 mV, in VM cells at +20 mV the I_{Ca} component was −436.7 ± 105.2 pA (17/17 cells) with τ_f 19.1 ± 8.4 msec and τ_s 112 ± 15.4 msec, whereas in P cells at +18.8 mV the I_{Ca} component was −96.8 ± 44.5* pA (present in 6/17 cells) with τ_f 11.4 ± 6.3 msec and τ_s 157.6 ± 61.2* msec.

I-V relation during slow depolarizing and repolarizing ramps in myocardial and Purkinje cells

Because in VM cells the sustained current at the end of depolarizing steps was larger at potentials negative to I_{K1} peak and smaller at positive potentials than in P cells (Fig. 4), the steady state I-V relation was studied during slowly depolarizing and repolarizing ramps in the two tissues.

In Figure 6A, in the P cell during 6.5 mV sec^{-1} depolarizing ramp, the outward current increased gradually less to stop increasing altogether between point 1 (−58 mV, I_{K1} peak) and point 2 (−30.7 mV). On further depolarization between points 2 and 3, the outward current increased markedly and before the ramp peak, underwent an enhancement (shaded area, the "bulge"; Du and Vassalle 1999). During the repolarizing ramp, the outward current initially decreased more rapidly, but 16 sec after the ramp peak it was similar to 16 sec before (at I_{K1} peak) (292 and 275 pA, respectively).

In Figure 6B, in the VM cell, the outward current also increased gradually less as a function of depolarization, but at point 1 (−48 mV, I_{K1} peak) the outward current was 179% larger than in the P cell. Also, a distinct NS region began at point 1 and was followed (change in slope) by an I_{Ca} component that peaked at +2 mV (point 2). Between points 2 and 3, the current reincreased in an outward direction, but it was much smaller than in the P cell. Furthermore, there was no enhancement of the outward current (no "bulge") and at the ramp peak (point 3) the current was less outward than at point 1, in sharp contrast with the P cell.

During the repolarizing ramp, the outward current decreased much less than in the P cell and it was less inward (star) than at point 2. The outward current reincreased in the positive slope (PS) region to a peak value (786 pA) similar to that of I_{K1} peak (769 pA). Past the peak of I_{PS}, the outward current underwent a progressively quicker decrease as a function of repolarization.

In Table 5, with respect to P cells, in VM cells I_{K1} was larger (*) and peaked at a less negative potential (*). I_{NS} was larger (*), was more frequently present and peaked at less negative value (*). The I_{Ca} component was larger when measured from its beginning to its peak and when the I_{Ca} peak was compared to the symmetrical peak during repolarizing ramp. The outward current began to reincrease ("I_{to} start") at less negative potential (*) to reach a value at the ramp peak ("I_{to}") which was smaller (*) (although it was similar when measured with respect to I_h).

During the repolarizing ramp, the decrease of outward current (I_{repol}) was smaller (*) and peaked at less negative potential (*). I_{PS} (consistently present in VM but not in P cells) began at a more positive potential (*) and it was much larger (*) as it was (*) when measured with respect to I_h although less so. In VM cells, I_{K1} peak was similar to I_{PS} peak as it was in P cells at I_{PS} peak (or at the value at which the outward current began to decrease rapidly). This suggests that in neither tissue the Na^+ currents contributed to I_{K1} or I_{PS} peaks.

Thus, with slow ramps, with respect to P cells, in VM cells: (1) I_{K1} peak was much larger and peaked at a less negative potential; (2) I_{NS} was larger and peaked at less negative potentials; (3) I_{Ca} component was larger; (4) the outward current enhancement prior to ramp peak (the "bulge") was absent; (5) the outward current at ramp

peak was much smaller (but less so when compared to I_h); (6) during repolarizing ramps, the smaller I_{repol} declined much less; (7) I_{PS} was present more frequently, was larger and with a more positive beginning, and (8) I_{PS} and I_{K1} peaks were similar, both being larger than the ramp peak current.

Slope conductance changes during slow ramps in Purkinje and myocardial cells

If, during depolarization, the gradually smaller increase in outward current is due to the inward rectification of I_{K1} channel, the slope conductance should decrease accordingly. To find out, the slope conductance was measured by superimposing small hyperpolarizing voltage pulses on the parent ramp (protocol in Fig. 6C).

In the P cell (Fig. 6D), the amplitude of the pulse current at V_h −80 mV decreased gradually on depolarization to reach a minimal value at −44 mV, just prior the beginning of a small NS region. During I_{NS}, the pulse current reversed polarity and reincreased. With further depolarization, the pulse current decreased again, became once more negative and reincreased in amplitude. During the repolarizing ramp, similar events occurred in reverse order, including a smaller increase in slope conductance during a rather small I_{PS}.

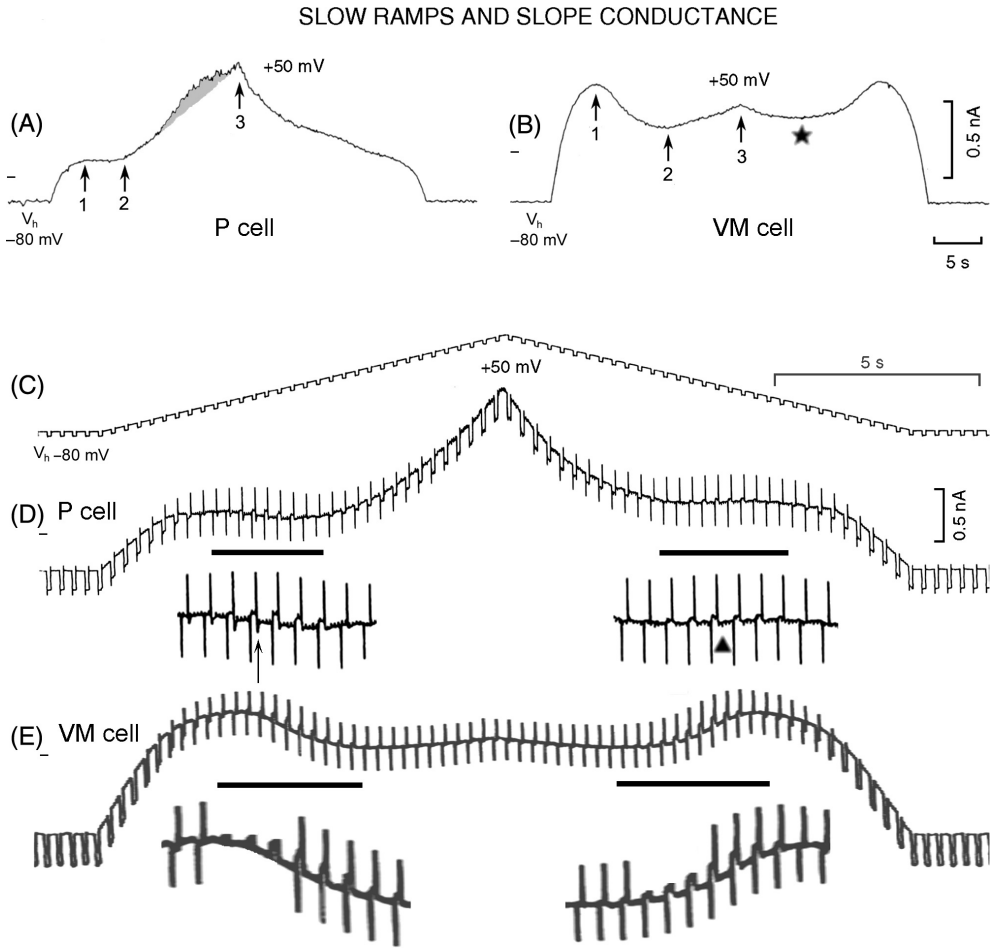

Figure 6. I-V relation and changes in slope conductance during slow ramps in P and VM cells. A 6.5 mV sec^{-1} depolarizing and repolarizing ramp was applied to a P cell (A) and to a VM cell (B). Point 1 indicates the I_{K1} peak, point 2 the beginning of increasing outward current, and point 3 the current at ramp peak. In A, the shaded area indicates the enhancement of the outward current ("the bulge"). In B, the asterisk indicates the transition between the decreasing outward current and the beginning of I_{PS}. Hyperpolarizing voltage pulses (amplitude 7 mV, duration 200 msec, rate 90 min^{-1}; C) were superimposed on the parent ramp to measure slope conductance. In D (P cell) and E (VM cell) (same heart but different from that for A and B), the horizontal lines indicate the sections of current records shown at higher gain underneath. In D, the upward vertical arrow points to an inward transient after the reversed pulse current and the triangle points to its absence. In the enlarged sections of VM trace, some of the capacity spikes have been deleted for a better visualization of the increase and reversal of pulse current in the NS and PS regions.

Table 5. Currents during 6.5 mV sec^{-1} ramp in VM and P cells.

n 15, Param	VM cells	P cells	Δ (mV or %)
V_h (mV)	−80.6 ± 0.6	−81.3 ± 0.9	−0.7 mV
I_{K1} peak (pA)	965 ± 124	465 ± 57*	+107.5%
I_{K1} peak (mV)	−44.2 ± 1.7	−50.1 ± 1.2*	5.9 mV
I_{NS} (pA)	−218 ± 31 (14/15)	−45.6 ± 12.0* (10/15)	+379.3%
I_{NS} peak (mV)	−3.9 ± 3.1	−23.2 ± 5.1*	19.3 mV
I_{Ca} start (mV)	−11.6 ± 5.2	−4.4 ± 3.0	−7.2 mV
I_{Ca} (pA)	−39.9 ± 17.5 (6/15)	−20.1 ± 9.6 (4/15)	+98.5%
I_{Ca} peak (mV)	−5.1 ± 4.7	−10.5 ± 7.2	5.4 mV
Δ (pA)	−51.9 ± 6.9 (15/15)	−29.8 ± 9.3 (7/15)	+74.1%
I_{to} start (mV)	0.64 ± 2.1	−19.2 ± 3.7*	19.8 mV
I_{to} (pA)	109 ± 14	436 ± 62*	−75%
$I_{ramp\ peak}-I_h$ (pA)	812 ± 114	863 ± 71	−5.9%
I_{repol} (pA)	64.7 ± 10.8	396.4 ± 62.2*	−83.6%
I_{repol} peak (mV)	8.8 ± 2.6	−15.9 ± 4.6*	24.7 mV
I_{PS} start (mV)	8.9 ± 2.6	−5.6 ± 2.7*	14.5 mV
I_{PS} peak (pA)	197.0 ± 28.4 (15/15)	36.0 ± 19.0* (5/15)	+447.2%
I_{PS} peak (mV)	−44.4 ± 1.6	−52.1 ± 1.8	7.7 mV
I_{PS} peak−I_h (pA)	981 ± 124	428 ± 68*	+53.3%

n 15, number of cells studied; Δ (mV or %), difference in mV or percent of VM cells data with respect to P cells data; I_{K1} peak (pA), amplitude of I_{K1} peak in pA, measured as the difference from I_h; I_{K1} peak (mV), voltage in mV at which I_{K1} peaked; I_{NS} (pA), current amplitude in pA during the negative slope region; I_{NS}, peak (mV), voltage in mV of I_{NS} peak; I_{Ca} start (mV), beginning of I_{Ca} component in mV determined as the departure of current trace from I_{NS} peak; I_{Ca} (pA), amplitude of I_{Ca} component in pA as the difference between its beginning and its peak; I_{Ca} peak (mV), peak in mV of I_{Ca}; Δ (pA), difference in pA between I_{Ca} peak during depolarization and minimum outward current preceding the beginning of I_{PS} on repolarization; I_{to}, start (mV), voltage in mV at which the increasing outward current started at I_{NS} or I_{Ca} peaks; I_{to} (pA), amplitude of outward current in pA measured between its beginning and ramp peak; $I_{ramp\ peak}-I_h$ (pA), outward current at ramp peak measured as difference from I_h; I_{repol} (pA), amplitude in pA of the outward current between ramp peak and its smallest value prior to the beginning of I_{PS}; I_{repol} peak (mV), voltage in mV at which the outward current was smallest prior to I_{NS} beginning; I_{PS} start (mV), voltage in mV at which I_{PS} began; I_{PS} peak (pA), current in pA at I_{PS} peak, measured as difference between its beginning and its peak; I_{PS} peak (mV), voltage in mV at which PS region peaked; I_{PS} peak−I_h (pA), current in pA measured as difference between I_{NS} peak and I_h; V_h (mV), holding potential in mV; Param, parameters measured; VM cells, data from ventricular myocardial cells; P cells, data from Purkinje cells; *statistically significant difference between P and VM cells data.

The sections of the traces labeled with a horizontal line are shown underneath at higher gain for a better visualization of pulse current changes. The arrow under the magnified trace points to a small inward component that followed the outward pulse current: such an inward component was not present during the repolarizing ramp (triangle) or in the VM cells (see below), suggesting that the brief hyperpolarizing step allowed an increased availability of sodium channels.

In the VM cell (Fig. 6E), at V_h the amplitude of the pulse current was larger (+72%) than in the P cell. The pulse current decreased on depolarization to become minimal at −31 mV, reversed polarity during I_{NS} and increased to a maximum at −14 mV, decreased again and then underwent a much smaller increase than in the P cell during the remainder of the ramp. During the repolarizing ramp, similar events occurred in reverse order, including an increase in slope conductance during I_{PS}.

In VM cells (n = 11, of which 3 from the same hearts as P cells) the pulse current amplitude varied as follows: −381.7 ± 34.6 pA at V_h −81.8 mV, 0 pA at I_{K1} peak (−39.2 mV), +75.6 ± 19.8 pA at the −14.3 mV reversal peak during I_{NS} (which was −310.3 ± 80.3 pA, 11/11 cells), and −16.7 ± 4.9 pA at ramp peak. With repolarizing ramps, the pulse current amplitude was −107.1 ± 18.5 pA at +13.7 mV, +84.6 ± 22.0 pA at −16.1 mV during I_{PS}, and 3.9 ± 3.9 pA (10/11 cells) at I_{PS} peak (which was at −42.5 ± 1.7 mV). I_{K1} and I_{PS} peaks were 1208 ± 207 and 1224 ± 210 pA, respectively.

In P cells (n = 21), the pulse current amplitude varied as follows. It was −190.8 ± 20.1* pA at V_h −88.5 mV and 0 pA at I_{K1} peak (−47.1 ± 1.5* mV). I_{NS} was 7.2 ± 4.4* pA and was present only in 3/21 cells. The pulse current amplitude was −110.0 ± 11.7* pA at the ramp peak. During the repolarizing ramp, the pulse current amplitude was −71.4 ± 6.8 pA at +17.7 mV (* with respect to −119 pA at +20.1 mV during depolarization) and 2.5 ± 2.2 pA at the potential where the final faster depolarization began (I_{PS} was present in 2/21 cells).

In the cells from the same three hearts with the same −83.3 mV V_h, similar results were obtained in that in VM cells the pulse current amplitude at V_h was larger by +88.8%, the pulse current fell to 0 pA at a less negative potential, I_{NS} was +923% larger, the pulse current at ramp peak smaller by −87.5%, the reversed pulse current during I_{PS} was 73 pA (there was no I_{PS} in P cells).

Thus, with respect to P cells, in VM cells the pulse current: (1) was larger at V_h (+100.0%*); (2) fell to a minimum at the 7.9 mV* less negative I_{K1} peak; (3) consistently reversed and reincreased during I_{NS}; (4) fell again by I_{NS} end and reincreased but much less (−84.8% * than P cells at the ramp peak; and (5) during the repolarizing ramp, the smaller VM conductance underwent the converse changes, reincreasing during I_{PS}.

Current during fast ramps in myocardial and Purkinje cells

As with the 6.5 mV sec^{-1} ramps, the Na^+ channels would be inactivated, depolarizing and repolarizing ramps with progressively steeper slopes were applied to VM and P cells.

In Figure 7, 260 mV sec^{-1} ramp, with respect to the P cell (Fig. 7A), in the VM cell (Fig. 7B) at point 1 I_{K1} peak was much larger and less negative. In both P and VM cells, immediately after I_{K1} peak, a slowly increasing I_{Na3} (shaded areas labeled by downward arrows) preceded the activation of I_{Na1}, as expected from the more negative threshold of I_{Na3} (see Figs. 1 and 3). In the P cell, I_{NS} (empty circle) peaked at point 2 and was followed by an

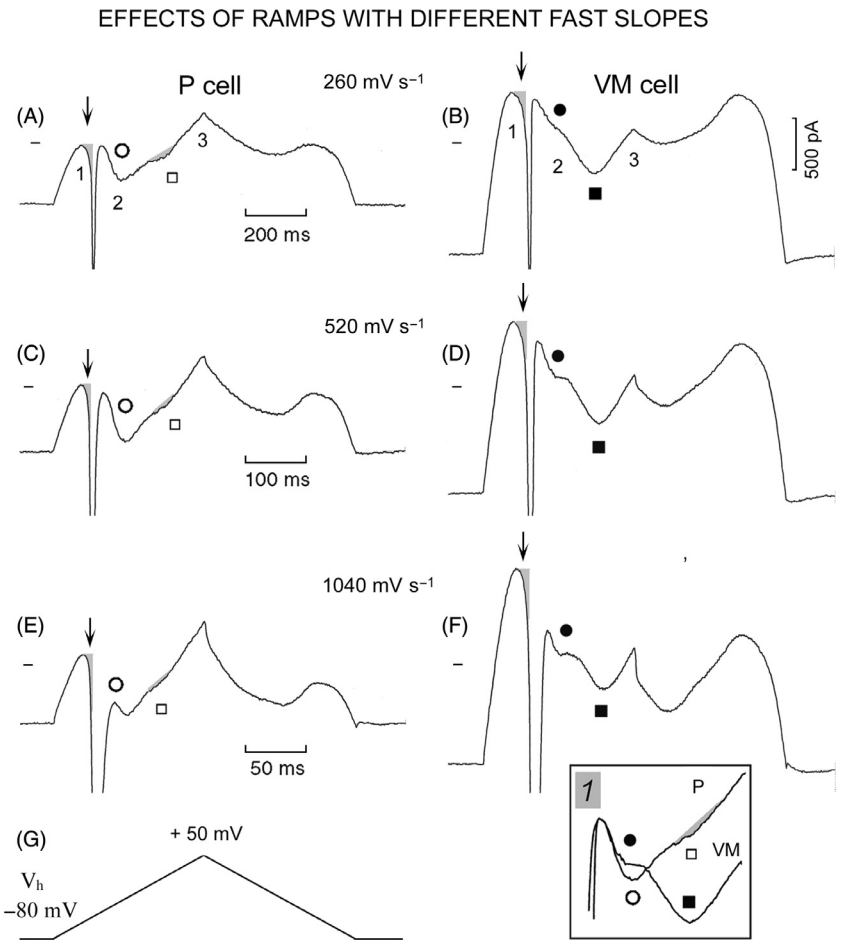

Figure 7. I-V relation during steep ramps in P and VM cells. The 260, 520, and 1040 mV sec^{-1} ramps were applied from V_h −80 to +50 mV (G) to a P cell (A, C, and E, respectively) and a VM cell (B, D, and F, respectively). The numbers 1, 2, and 3 label the peaks of I_{K1}, of I_{NS}, and of the ramp, respectively. I_{NS} is labeled by empty circles in the P cell and by filled circles in the VM cell. The inward component attributable to I_{Ca} is labeled by empty squares and small shaded areas in the P cell, and by filled squares in the VM cell. In VM cells, I_{Ca} was measured from its beginning (taken as the point at which the slope of I_{NS} met the backward extrapolation of I_{Ca}) and I_{Ca} peak. The downward vertical arrows point to the slowly increasing inward current (shaded areas) preceding the activation of I_{Na1}. In inset 1, the traces from C and D were superimposed by the end of I_{Na1} inactivation. In both cells, I_{Na1} was cut off by the saturation of the amplifier at −10 nA.

increasing outward current. A very shallow inward component, peaking at +12 mV, appeared as an "indentation" on the increasing outward current (empty square and small shaded area). In the VM cell, I_{NS} (filled circle) was smaller and was followed by a large inward component (filled square) which peaked at +17 mV, as expected from a larger I_{Ca} component.

Similar but not identical results were obtained during the 520 mV sec^{-1} (Fig. 7C and D) and 1040 mV sec^{-1} (Fig. 7E and F) ramps. I_{K1} peak increased in magnitude with the steeper ramps both in P and VM cell, still being much smaller in the P cell. In both cells, the steeper ramp slope caused I_{Na1} to inactivate closer to the end of I_{NS}. As usual, the outward current at ramp peak (point 3) was larger than I_{K1} peak (point 1) in the P cell (Fig. 7C and E) whereas it was smaller in the VM cell (Fig. 7D and F). I_{NS} of the P cell (Fig. 7C) and that of the VM cell (Fig. 7D) were superimposed by the end of I_{Na1} inactivation in Figure 7 inset 1. While I_{NS} was larger in the P cell, the subsequent I_{Ca} component was much larger (filled square) in the VM cell.

On repolarization, in the P cell the outward current decreased more and peaked at more negative values than in the VM cell. In both cells, on repolarization with steeper ramps the decrease in outward current was faster initially and it was larger. Also, I_{PS} started from a less outward value and, on that account, I_{PS} peak became smaller than the I_{K1} peak.

As shown in Table 6, during the 260 mV sec^{-1} ramp with respect to P cells, in VM cells I_{K1} peak was larger (*) and less negative (*), I_{NS} was smaller and its peak was less negative (*). I_{Na3} amplitude was somewhat greater, I_{Na1} threshold was less negative (*), I_{Na1} amplitude was similar (there was I_{Na1} in 14/17 VM cells and in 8/17 P cells).

The I_{Ca} component was larger (*) (there was a measurable I_{Ca} component in15/17 VM cells and in 3/17 P cells). The outward current between I_{Ca} and ramp peaks ("I_{to}") began at a more positive potential (*) and was smaller (*). When the ramp peak current was measured as the difference from I_h, I_{to} was smaller (*) but less so, due to the larger I_{K1} upon which the ramp peak current was superimposed.

Table 6. Currents during the 260 mV sec^{-1} ramp in VM and P cells.

n 17, Param	VM cells	P cells	Δ (mV or %)
V_h (mV)	−80.6 ± 0.6	−81.8 ± 1.0	−1.2 mV
I_{K1} peak (pA)	913 ± 101	477 ± 56.8*	+91.4%
I_{K1} peak (mV)	−52.1 ± 1.0	−57.3 ± 1.0*	5.2 mV
I_{NS} (pA)	−216.6 ± 26.3	−340.5 ± 44.3*	−36.3 %
I_{NS} peak (mV)	−14.0 ± 1.6	−26.5 ± 1.5*	12.5 mV
I_{Na3} (pA)	−941 ± 119 (14/17)	−733 ± 89 (8/17)	+28.3%
I_{Na1}Th (mV)	−40 ± 1.5	−47.3 ± 1.8*	−7.2 mV
I_{Na1} (pA)	−7298 ± 842 (14/17)	−6978 ± 850 (8/17)	+4.5%
End I_{Na1} (pA)	910 ± 109 (14/17)	324 ± 64* (8/17)	+180.8%
End I_{Na1} (mV)	−34.2 ± 1.5	−39.5 ± 1.5*	5.3 mV
I_{Ca} start (mV)	−9.2 ± 2.0	−15 ± 1.0*	5.8 mV
I_{Ca} (pA)	−108.3 ± 24.2 (15/17)	−19.6 ± 11.6* (3/17)	+452.5%
I_{Ca} peak (mV)	14.0 ± 0.9	−3.3 ± 3.7*	17.3 mV
I_{to} start (mV)	13.7 ± 0.9	−21.3 ± 2.8*	35 mV
I_{to} (pA)	206.0 ± 25.3 (17/17)	1270 ± 166* (17/17)	−83.7%
$I_{ramp\ peak}-I_h$ (pA)	783 ± 78 (17/17)	1373 ± 166* (17/17)	−42.9%
I_{repol} (pA)	123.5 ± 22	967 ± 139*	−87.2%
I_{repol} peak (mV)	7.2 ± 3.2	−15.9 ± 1.6*	23.1 mV
I_{PS} start (mV)	3.3 ± 3.2	−17.2 ± 1.7*	20.4 mV
I_{PS} (pA)	214 ± 29.8 (17/17)	64.6 ± 13.2* (15/17)	+231.2%
I_{PS} peak (mV)	−45.2 ± 1.6	−46.7 ± 2.9	1.5 mV
I_{PS} peak−I_h (pA)	895 ± 103 (17/17)	395 ± 58* (15/17)	+126.5%

End I_{Na1} (pA), Amplitude in pA of the current at the end of I_{Na1} inactivation; End I_{Na1} (mV), voltage in mV of the current at the end of I_{Na1} inactivation; V_h (mV), holding potential in mV; Param, parameters measured; VM cells, data from ventricular myocardial cells; P cells, data from Purkinje cells; I_{Na1} Th (mV), threshold potential in mV of I_{Na1}; I_{Na3} (pA), amplitude in pA of I_{Na3} measured as the difference between its peak and the end of the step; I_{Na1} (pA), amplitude in pA of I_{Na1}; Numbers in parenthesis (e.g., 14/17), number of cells in which the parameter was present over the total number of cells studied; *statistically significant difference between P and VM cells data. Other explanations as in the legend of Table 5.

The I_{K1} peak was similar to the current at the end of I_{Na1} inactivation both in the VM cells (0.003%) and in the eight P cells in which I_{Na1} was present (I_{K1} peak 389.1 pA and at the end of I_{Na1} 324.6 pA, difference not statistically significant). These results are consistent with the elimination of the slow inactivation of I_{Na3} by I_{Na1} in both tissues. At the end of I_{Na1}, the voltage was less negative in VM cells (*), reflecting the less negative I_{Na1} threshold (*).

In VM cells, with respect to the 260 mV sec^{-1} ramp, the 520 (Table 7) and 1040 mV sec^{-1} (Table 8) *depolarizing* ramps induced the following changes, respectively: peak I_{K1} +5.4% and +18.5%, I_{Na3} +75.0%* and +132%*, I_{Na1} +39.3% and +53.0%*, I_{NS} +28.3% and +86.9%,* I_{Ca} component +10.0% and +3.0%, "I_{to}" +8.2% and +7.8%, and $I_{ramp\ peak}-I_h$, +5.1% and +12.8%.

In P cells, with respect to the 260 mV sec^{-1} ramp, the 520 (Table 7) and 1040 mV sec^{-1} (Table 8) ramps induced the following changes, respectively: peak I_{K1} +8.5% and +28.7%, I_{Na3} +291.8%* and +376.8%*, I_{Na1} +187.5%* and +189.0%*, I_{NS} +60.5%* and +108.8%*, "I_{to}" +16.3% and +39.8%*, and $I_{ramp\ peak}-I_h$, +2.3% and +20.7%*.

Thus, in both VM and P cells the faster ramps increased I_{K1} peak, I_{Na3}, I_{Na1}, $I_{NS,}$ and $I_{ramp\ peak}$ when measured either from its beginning during the ramp or from I_h. The increase in I_{Na3} and in I_{NS} was larger in P cells, consistent with I_{Na3} role in I_{NS}.

Table 7. Currents during the 520 mV sec^{-1} ramp in VM and P cells.

n 17, Param	VM cells	P cells	Δ (mV or %)
V_h (mV)	−80.6 ± 0.5	−81.8 ± 0.9	−0.7 mV
I_{K1} peak (pA)	963 ± 108	518 ± 57*	+46.2%
I_{K1} peak (mV)	−52.3 ± 0.7	−58.3 ± 0.7*	6 mV
I_{NS} (pA)	−278 ± 36	−546 ± 48*	−49.0%
I_{NS}, peak	−18.1 ± 2.6	−22.4 ± 1.6	4.3 mV
I_{Na3} (pA)	−1458 ± 170 (17/17)	−1352 ± 175 (14/17)	+7.8%
I_{Na1}Th (mV)	−39.2 ± 1.2	−46.8 ± 1.2*	7.6 mV
I_{Na1} (pA)	−8373 ± 553 (17/17)	−9439 ± 352 (14/17)	−11.9%
End I_{Na1} (pA)	837 ± 113	381 ± 69*	+119.6%
End I_{Na1} (mV)	−32.6 ± 1.2	−38.5 ± 1.0*	5.9 mV
I_{Ca}, start (mV)	−4.9 ± 1.9	−11.5 ± 0.5*	6.6 mV
I_{Ca} (pA)	−119.2 ± 31.7 (16/17)	−16.4 ± 14.1* (2/17)	+626.8%
I_{Ca} peak (mV)	17.4 ± 0.9	−3.5 ± 7.5	20.9 mV
I_{to}, start (mV)	10.3 ± 3.4	−17.1 ± 2.0* (17/17)	27.4 mV
I_{to} (pA)	223 ± 27.0	1478 ± 173* (17/17)	−84.9%
$I_{ramp\ peak}-I_h$ (pA)	823 ± 88	1405 ± 167	−41.4%
I_{repol} (pA)	198 ± 32	1169 ± 144*	−83.0%
I_{repol} peak (mV)	3.1 ± 3.6	−16.6 ± 2.0*	19.4 mV
I_{PS}, start (mV)	0.2 ± 3.7	−17.1 ± 1.8*	17.3 mV
I_{PS} (pA)	219 ± 34	122 ± 20	79.5%
I_{PS} peak (mV)	−45.3 ± 1.7	−49.8 ± 1.0*	4.5 mV
I_{PS} peak−I_h (pA)	850 ± 105	349 ± 55*	+143.5%

n, number of cells studied; Δ (mV or%), difference in mV or percent of VM cells data with respect to P cells data; I_{K1} peak (pA), amplitude of I_{K1} peak in pA, measured as the difference from I_h; I_{K1} peak (mV), voltage in mV at which I_{K1} peaked; I_{NS} (pA), current amplitude in pA during the negative slope region; I_{NS}, peak (mV), voltage in mV of I_{NS} peak; I_{Na1} Th (mV), voltage at which I_{Na1} began; I_{Na1} (pA), amplitude in pA of I_{Na1}; I_{Ca} start (mV), beginning of I_{Ca} component in mV determined as the departure of current trace from I_{NS} peak; I_{Ca} (pA), amplitude of I_{Ca} component in pA as the difference between its beginning and its peak; I_{Ca} peak (mV), peak in mV of I_{Ca}; I_{to}, start (mV), voltage in mV at which the increasing outward current started at I_{NS} or I_{Ca} peaks; I_{to} (pA), amplitude of outward current in pA measured between its beginning and ramp peak; $I_{ramp\ peak}-I_h$ (pA), outward current at ramp peak measured as difference from I_h; I_{repol} (pA), amplitude in pA of the outward current between ramp peak and its smallest value prior to the beginning of I_{PS}; I_{repol} peak (mV), voltage in mV at which the outward current was smallest prior to I_{NS} beginning; I_{PS} start (mV), voltage in mV at which I_{PS} began; I_{PS} (pA), current in pA at I_{PS} peak, measured as difference between its beginning and its peak; I_{PS} peak (mV), voltage in mV at which PS region peaked; I_{PS} peak−I_h (pA), current in pA measured as difference between I_{NS} peak and I_h; End I_{Na1} (pA), amplitude in pA of the current at the end of I_{Na1} inactivation; End I_{Na1} (mV), voltage in mV of the current at the end of I_{Na1} inactivation; V_h (mV), holding potential in mV; Param, parameters measured; VM cells, data from ventricular myocardial cells; P cells, data from Purkinje cells; I_{Na3} (pA), amplitude in pA of I_{Na3} measured as the difference between its peak and the end of the step; Numbers in parenthesis (e.g., 17/17), number of cells with the parameter present over the total number of cells studied; *statistically significant difference between P and VM cells data.

As for the *repolarizing* ramps, with respect to P cells, in VM cells during the 260 mV sec^{-1} ramp (Table 6), the decreasing outward current was smaller (*) and peaked at a more positive potential (*). I_{PS} began at a less negative potential (*) and was larger (*). It was larger also when measured as the difference from I_h (*).

In VM cells, with respect to the 260 mV sec^{-1} repolarizing ramp, the 520 (Table 7) and 1040 mV sec^{-1} (Table 8) repolarizing ramps induced the following changes, respectively: I_{repol} larger by +60.3% and by +220%*, the difference in initiation of I_{PS} 3.1 and 2.1 mV, difference in voltage of I_{PS} peak 0.1 and 2 mV, amplitude of I_{PS} peak +0.2% and +4.2% and, when compared to I_h, −5.0% and −18.1%. Therefore, on repolarization the decrease of I_{repol} (but not I_{PS}) was sensitive to the repolarizing ramp slope.

In P cells, with respect to the 260 mV sec^{-1} repolarizing ramp, the 520 (Table 7) and 1040 mV sec^{-1} (Table 8) repolarizing ramps induced the following changes, respectively: I_{repol} larger by 20.8% and by 57.3%*, difference in I_{PS} initiation 0.1 and 1.8 mV, difference in voltage of I_{PS} peak −3.1 and −3.7 mV, amplitude of I_{PS} peak +88.8%* mV and +152.3%* and, when measured from I_h, −11.6% and −38.2%*.

Therefore, in P cells I_{Na3} and I_{NS} became greater with faster depolarizing ramps, suggesting that sodium currents play a larger role in NS region of P cells than in that of VM cells. Also, during repolarizing ramp, the outward

Table 8. Currents during the 1040 mV sec^{-1} ramp in VM and P cells.

n 17, Param	VM cells	P cells	Δ (mV or %)
V_h (mV)	−80.6 ± 0.5	−81.8 ± 0.9	1.2 mV
I_{K1} peak (pA)	1082 ± 113	614 ± 60*	+76.2%
I_{K1} peak (mV)	−52.2 ± 0.7	−58.0 ± 0.7*	5.8 mV
I_{NS} (pA)	−405 ± 57	−710 ± 74*	−42.9%
I_{NS} peak (mV)	−16.2 ± 2.6	−19.8 ± 1.4	3.6 mV
I_{Na3} (pA)	−1986 ± 132	−1645 ± 199	+20.7%
I_{Na1} Th (mV)	−38.3 ± 1.1	−47.1 ± 0.9*	8.8 mV
I_{Na1} (pA)	−9197 ± 393 (17/17)	−9491 ± 280 (16/17)	−3.09%
End I_{Na1} (pA)	863 ± 105 (17/17)	351 ± 69* (16/17)	+145.8%
End I_{Na1} (mV)	−27.9 ± 1.5	−30.8 ± 4.4	2.9 mV
I_{Ca} start (mV)	−0.6 ± 1.7	−8.0 ± 0.0	7.2 mV
I_{Ca} (pA)	−111.6 ± 28.6 (14/17)	−19.5 ± 18.0* (2/17)	+472%
I_{Ca} peak (mV)	20.9 ± 1.1	−4.0 ± 1*	24.9 mV
I_{to} start (mV)	14.0 ± 4.0	−14.1 ± 3.25*	28.1 mV
I_{to} (pA)	222 ± 28	1776 ± 187*	−87.5%
$I_{ramp\ peak}-I_h$ (pA)	884 ± 85	1658 ± 172	−46.6%
I_{repol} (pA)	396 ± 50	1522 ± 158*	−73.9%
$I_{repol\ peak}$ (mV)	10 ± 3.3	−16.7 ± 2.0*	26.7 mV
I_{PS} start (mV)	5.4 ± 3.6	−18.9 ± 1.9*	24.3 mV
I_{PS} (pA)	223 ± 40	163 ± 24 (15/17)	+36.8%
I_{PS} peak (mV)	−47.2 ± 1.7	−50.4 ± 1.0	3.2 mV
I_{PS} peak−I_h (pA)	733 ± 100	244 ± 47*	+200.4%

n, number of cells studied; Δ (mV or%), difference in mV or percent of VM cells data with respect to P cells data; I_{K1} peak (pA), amplitude of I_{K1} peak in pA, measured as the difference from I_h; I_{K1} peak (mV), voltage in mV at which I_{K1} peaked; I_{NS} (pA), current amplitude in pA during the negative slope region; I_{NS}, peak (mV), voltage in mV of I_{NS} peak; I_{Na1} Th (mV), voltage at which I_{Na1} began; I_{Na1} (pA), amplitude in pA of I_{Na1}; I_{Ca} start (mV), beginning of I_{Ca} component in mV determined as the departure of current trace from I_{NS} peak; I_{Ca} (pA), amplitude of I_{Ca} component in pA as the difference between its beginning and its peak; I_{Ca} peak (mV), peak in mV of I_{Ca}; I_{to}, start (mV), voltage in mV at which the increasing outward current started at I_{NS} or I_{Ca} peaks; I_{to} (pA), amplitude of outward current in pA measured between its beginning and ramp peak; $I_{ramp\ peak}-I_h$ (pA), outward current at ramp peak measured as difference from I_h; I_{repol} (pA), amplitude in pA of the outward current between ramp peak and its smallest value prior to the beginning of I_{PS}; $I_{repol\ peak}$ (mV), voltage in mV at which the outward current was smallest prior to I_{NS} beginning; I_{PS} start (mV), voltage in mV at which I_{PS} began; I_{PS} (pA), current in pA at I_{PS} peak, measured as difference between its beginning and its peak; I_{PS} peak (mV), voltage in mV at which PS region peaked; I_{PS} peak−I_h (pA), current in pA measured as difference between I_{PS} peak and I_h; End I_{Na1} (pA), Amplitude in pA of the current at the end of I_{Na1} inactivation; End I_{Na1} (mV), voltage in mV of the current at the end of I_{Na1} inactivation; V_h (mV), holding potential in mV; Param, parameters measured; VM cells, data from ventricular myocardial cells; P cells, data from Purkinje cells; I_{Na3} (pA), amplitude in pA of I_{Na3} measured as the difference between its peak and the end of the step; Numbers in parenthesis (e.g., 17/17), number of cells in which the parameter was present over the total number of cells studied; *statistically significant difference between P and VM cells data. Other explanations as in the legend of Table 7.

current decreased more with faster ramps in both P and VM cells. With faster ramps, starting from a lower value, I_{PS} increased in P cells, but decreased when measured as the difference from I_h.

Differences in I_{NS} in Purkinje versus myocardial cells

A decrease of V_h from −90 mV to −60 mV markedly decreased the amplitude of I_{NS} in P cells (Rota and Vassalle 2003; Vassalle et al. 2007; present results), but not in VM cells as measured using the sustained current at the end of depolarizing steps (Fig. 4). The finding suggests that the Na^+ current may play a predominant role in the mechanisms underlying I_{NS} in P but not in VM cells. This was tested by applying ramps from different V_h.

In Figure 8A, in a VM cells, V_h was progressively decreased by 1 mV and 520 mV sec^{-1} ramps were applied from V_h indicated above the I_h trace (−60 to −43 mV). At V_h −60 mV (top *A* trace), I_{Na1} was truncated at −10 nA and I_{NS} was followed by I_{Ca} component (−151 pA, as indicated above the trace) peaking at +22 mV. With V_h −54 mV, I_{Na1} was still larger than −10 nA, but beginning with V_h –53 mV, I_{Na1} gradually

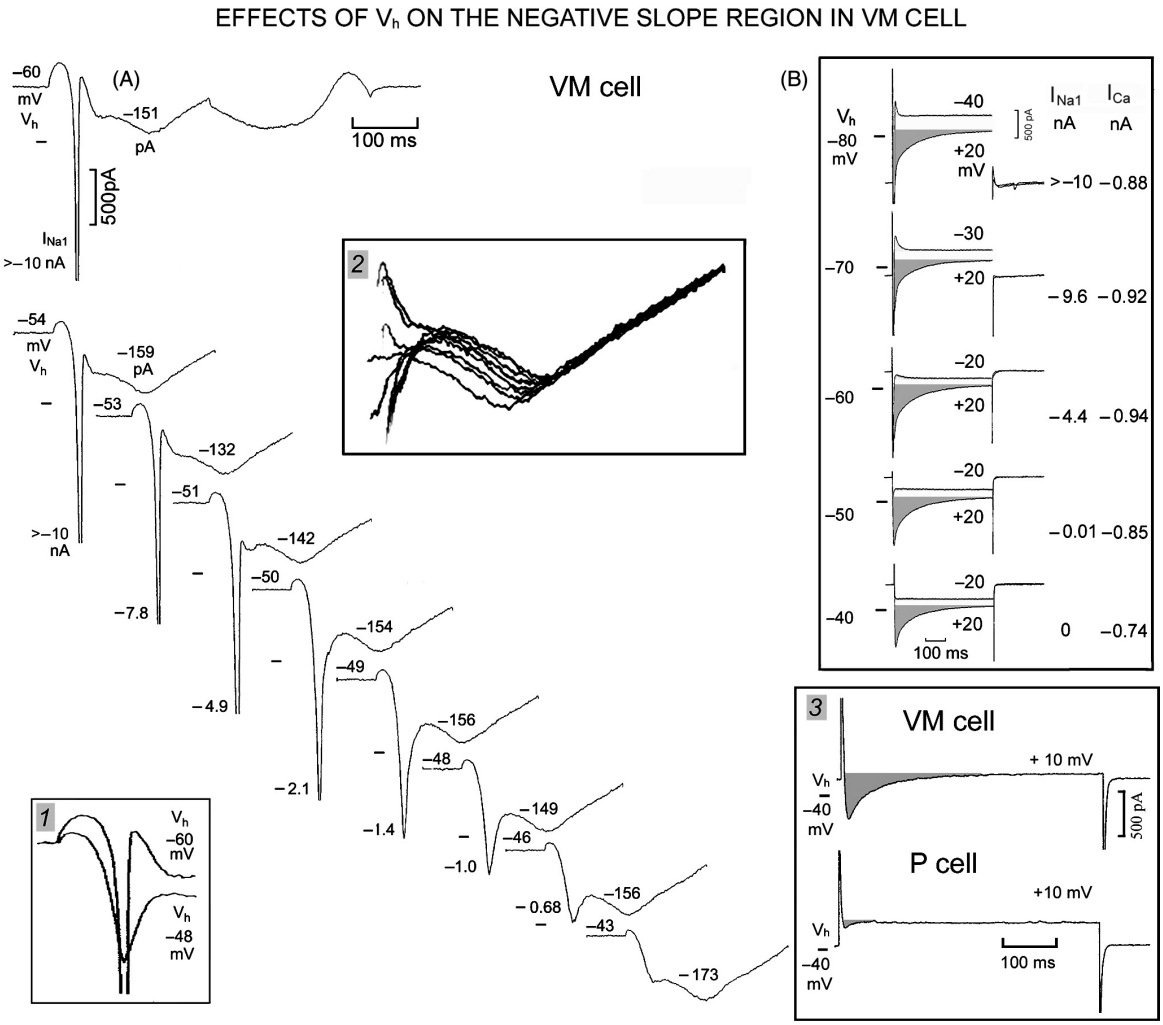

Figure 8. Persistence of NS region and of I_{Ca} with ramps from lower holding potentials in VM cells. In A, 520 mV sec^{-1} ramps were applied from the V_h indicated above I_h (−60 to −43 mV in 1 mV decrements; not all traces shown). I_{Na1} amplitude in nA is indicated next to the tip of I_{Na1} traces. In inset 1, the traces with V_h −60 and −48 mV have been superimposed. The amplitude in pA of I_{Ca} component (measured from its beginning to its peak) is indicated by the number above the traces. In inset 2, the superimposed traces show that I_{Ca} component was not affected by gradually smaller V_h. In B (from a different heart), depolarizing steps were applied from gradually lower V_h and the currents were superimposed at the indicated voltages. The amplitudes of I_{Na1} and of I_{Ca} (shaded area) are indicated in nA at the right hand of the traces. In inset 3, the voltage step was applied from V_h −40 to +10 mV in a VM and P cell.

decreased as indicated in nA next to the tip of I_{Na1} traces. Also, as I_{Na1} became much smaller, the activation and inactivation of the inward transient became slower, as illustrated in Figure 8 inset 1 by the superimposed V_h −60 and −48 mV traces. At V_h −43 mV (bottom trace), there was no apparent I_{Na1} and I_{NS} had an amplitude of −462 pA, a duration of 36 msec and a voltage range between −40 and −12 mV. Over the range of V_h tested, the I_{Ca} component peaked at ~+20 mV and its amplitude remained at ~−150 pA (see numbers above the I_{Ca} component traces and the superimposed traces in Figure 8 inset 2).

That the inward component positive to I_{NS} was due to I_{Ca} is supported by the results obtained with depolarizing steps applied from V_h −80, −70, −60, −50, and −40 mV (Fig. 8B). The amplitudes of I_{Na1} and of that of I_{Ca} (shaded areas) are indicated, respectively, in nA at the right hand of traces. I_{Na1} decreased gradually with the less negative V_h and disappeared with V_h −50 and −40 mV. Instead, the slowly inactivating current persisted even with V_h of −40 mV (albeit somewhat decreased) as expected for I_{Ca} (Isenberg and Klöckner 1982). In Figure 8 inset 3, depolarizing steps were applied from V_h −40 to +10 mV and show that I_{Ca} was far larger in the VM than in the P cell, as usual.

The results are consistent with Na^+ currents playing little role in I_{NS} of VM cells and also with I_{Ca} underlying the inward component that peaked at ~+20 mV (as well as the small indentation over a similar voltage range in P cells).

In Table 9, in VM cells fast ramps were applied from V_h −80 and −50 mV with the following changes. I_{K1} peak decreased (*) as the K1 channel rectified inwardly at lower V_h before the ramp was applied. I_{NS} was not affected whereas I_{Na1} markedly decreased (*). The I_{Ca} component was similar. The ramp peak current (I_{to}) increased (the ramp peak voltage being more positive), although it was smaller when measured as $I_{ramp\ peak}-I_h$ (*) due to the inward shift of the current with less negative V_h. I_{PS} and its peak voltage were similar. However, I_{PS} peak measured relative to I_h was 820 pA in control

Table 9. Less negative V_h of fast ramps markedly decreases I_{NS} and I_{PS} in P but not in VM cells.

Param	VM cells *n* 7	VM cells	P cells *n* 4	P cells
V_h (mV)	−80 ± 0	−50 ± 0	−82.5 ± 2.5	−55.0 ± 2.8
I_{K1} peak (pA)	999 ± 223	92 ± 19*	270 ± 57	53.0 ± 15.5*
I_{K1} peak (mV)	−47.7 ± 4.4	−41.5 ± 2.8	−60 ± 3.4	−47.0 ± 2.8*
I_{NS} (pA)	−388 ± 75	−246 ± 46	−261 ± 91	−10.5 ± 6.5 (2/4) *
I_{NS} peak (mV)	−9.3 ± 4.7	−22.7 ± 3.4	−26.3 ± 3.0	−35.8 ± 6.3 (2/4)
I_{Na1} (pA)	−7988 ± 1170	−298 ± 87*	−9334 ± 665	−123 ± 123 (1/4) *
I_{Ca} start (mV)	−7.5 ± 4.7	−7.1 ± 5.8	0 ± 0	0 ± 0
I_{Ca} (pA)	−184 ± 52	−183 ± 77	0 ± 0	0 ± 0
I_{Ca} peak (mV)	15.5 ± 10.3	13.6 ± 5.4	0 ± 0	0 ± 0
I_{to} start (mV)	5.6 ± 7.8	14.2 ± 4.6	−15.4 ± 12	−6.8 ± 17.7
I_{to} peak (pA)	341 ± 87	542 ± 132	1586 ± 579	1789 ± 667
$I_{ramp\ peak}-I_h$ (pA)	842 ± 154	284 ± 98*	1597 ± 565	1826 ± 677
I_{repol} (pA)	192 ± 53	511 ± 104*	1420 ± 582	1831 ± 679
$I_{repol\ peak}$ (mV)	8.6 ± 7.5	−5.6 ± 5.2	−31.1 ± 5.3	−30.9 ± 9.2
I_{PS} start (mV)	5.7 ± 8.0	4.4 ± 4.5	−28.8 ± 6.8	0 ± 0*
I_{PS} peak (pA)	214 ± 61	218 ± 63	36.0 ± 20 (3/4)	0 ± 0
I_{PS} peak (mV)	−39.2 ± 6.0	−41 ± 5.0	−50.5 ± 5.0	0 ± 0*
$I_{PS}-I_h$ (pA)	820 ± 198	−5.0 ± 15.2*	213 ± 81 (3/4)	24.6 ± 15*

n, number of cells studied; I_{K1} peak (pA), amplitude of I_{K1} peak in pA, measured as the difference from I_h; I_{K1} peak (mV), voltage in mV at which I_{K1} peaked; I_{NS} (pA), current amplitude in pA during the negative slope region; I_{NS}, peak (mV), voltage in mV of I_{NS} peak; I_{Na1} (pA), amplitude in pA of I_{Na1}; I_{Ca} start (mV), beginning of I_{Ca} component in mV determined as the departure of current trace from I_{NS} peak; I_{Ca} (pA), amplitude of I_{Ca} component in pA as the difference between its beginning and its peak; I_{Ca} peak (mV), voltage in mV at which I_{Ca} peaked; I_{to}, start (mV), voltage in mV at which the increasing outward current started at I_{NS} or I_{Ca} peaks; I_{to} peak (pA), amplitude of outward current in pA measured between its beginning and ramp peak; $I_{ramp\ peak}-I_h$ (pA), outward current at ramp peak measured as difference from I_h; I_{repol} (pA), amplitude in pA of the outward current between ramp peak and its smallest value prior to the beginning of I_{PS}; I_{repol} peak (mV), voltage in mV at which the outward current was smallest prior to I_{NS} beginning; I_{PS} start (mV), voltage in mV at which I_{PS} began; I_{PS} peak (pA), current in pA at I_{PS} peak, measured as difference between its beginning and its peak; I_{PS} peak (mV), voltage in mV at which PS region peaked; I_{PS} peak−I_h (pA), current in pA measured as difference between I_{PS} peak and I_h; V_h (mV), holding potential in mV; Param, parameters measured; VM cells, data from ventricular myocardial cells; P cells, data from Purkinje cells; *statistically significant difference between the data at the two V_h values either in VM or P cells.

and −5.0 pA* with the less negative V_h, reflecting the inward shift of I_{K1} with V_h −50 mV. In 6 of 7 of these experiments, V_h was also decreased by 1–2 mV with the results similar to those illustrated in Figure 8A.

In Table 9, in P cells, the same procedure decreased I_{K1} peak (*), I_{NS} (*), and I_{Na1} (*). I_{Ca} was not measurable (only small indentations) either in control or at less negative V_h. "I_{to}" and $I_{ramp\ peak}$–I_h increased but not significantly. Furthermore, I_{PS} was smaller than in VM cells by 83.1% with V_h −80 mV and was not present with V_h −50 mV.

In Table 10, with V_h −80 mV during the step to ~+20 mV I_{Ca} was larger in VM cells (328%*) and did not decrease with gradually lower V_h in either VM cells (−24.8%, −6.5%, +17.5% and −29.6%, respectively) nor in P cells. However, in the latter tissue the I_{Ca} values varied irregularly, possibly due to the far fewer of P cells displaying it. Instead, as reported in Table 2, during depolarizing steps from V_h −70, −60, −50, and −40 mV, in VM cells I_{Na1} decreased by −3.4%, −30.3%, −75.6%, and −99.3%, and in P cells by −3.7%, −20.1%, −65.9%, −93.5%, respectively.

Thus, with less negative V_h, I_{Na1} markedly decreased in both tissues during both ramps and depolarizing steps. In VM cells, I_{NS} and I_{PS} regions persisted even at V_h −50 mV. Instead, in P cells with V_h −80 mV, I_{PS} was much smaller than I_{NS} and, with V_h −50 mV, I_{NS} was markedly diminished and I_{PS} abolished. Furthermore, in VM cells I_{Ca} was consistently present with V_h −80 mV and did not decrease with V_h −50 mV. In P cells, I_{Ca} was either not apparent or it was a small inward indentation on the outward current.

The transient outward current I_{to} in Purkinje and myocardial cells

Some of differences between currents in P and VM cells in the −20 to +40 mV range (see Fig. 2) were analyzed by applying the depolarizing steps from V_h −80 and V_h −40 mV in the absence and presence of I_{to} blocker 4-aminopyridine.

In Figure 9A, in P cell, during the step from V_h −80 to −20 mV, I_{Na2} slowly decayed (arrow). A small outward peak appeared at the beginning of the step to 0 mV and progressively increased in size with more positive steps. In Figure 9B, in VM cell from a different heart, no decaying inward I_{Na2} was apparent and, instead, a smaller outward current grew in amplitude over the range −20 to +40 mV. The sustained current at the end of the steps was smaller than in P cell (note the different current calibration).

In the presence of 4-AP in the P cell (Fig. 9C) the peak I_{to} was abolished, the decaying I_{Na2} was larger at negative values, and the sustained current was reduced. In the VM cell (Fig. 9D), 4-AP abolished the peak I_{to} and reduced the sustained current. An inward transient was present at −20 mV which increased at +20 mV. Thus, at −20 mV in P cells the inward current was much larger, inactivated more slowly than the current in VM cell, and decreased markedly at + 20 mV.

In Figure 9 inset 1, V_h was decreased to −40 mV in order to inactivate I_{Na2} (Vassalle et al. 2007; Bocchi and Vassalle 2008; present results) but not I_{Ca} (Isenberg and Klöckner 1982). At V_h −40 mV, I_{to} channel is partially inactivated, mid-inactivation voltage being ~−35 mV (Du-

Table 10. I_{Ca} during depolarizing steps from different V_h.

V_h (mV)	Param	VM cells	P cells
−80	I_{Ca} peak (mV)	+19.4 ± 0.5	+18.8 ± 1.2
	I_{Ca} (pA)	−415 ± 101 (18/18)	−96.8 ± 44.6* (6/18)
	τ_f (msec)	17.9 ± 7.9	11.4 ± 6.3
	τ_s (msec)	107.8 ± 15.1	157 ± 61.2*
−70	I_{Ca} peak (mV)	19.4 ± 0.6	19.4 ± 0.6
	I_{Ca} (pA)	−312 ± 71 (15/16)	−18.9 ± 10.7* (3/16)
−60	I_{Ca} peak (mV)	19.3 ± 0.7	20.0 ± 0.0
	I_{Ca} (pA)	−388 ± 73 (15/15)	−8.8 ± 6.1* (2/15)
−50	I_{Ca} peak (mV)	20.0 ± 0.9	16.9 ± 1.5
	I_{Ca} (pA)	−488 ± 76 (16/16)	−9.1 ± 34.7* (5/16)
−40	I_{Ca} peak (mV)	20.0 ± 0.0	18.3 ± 1.6
	I_{Ca} (pA)	−292 ± 67 (10/10)	−87.3 ± 41.3* (3/6)

I_{Ca} peak (mV), voltage in mV at which the I_{Ca} was largest; I_{Ca} (pA), amplitude of I_{Ca} in pA measured from its peak to the end of the step; V_h (mV), holding potential in mV; Param, parameters measured; VM cells, data from ventricular myocardial cells; P cells, data from Purkinje cells; τ_f (msec) and τ_s (msec), fast and slow time constants, respectively, of I_{Ca} inactivation; Numbers in parenthesis (e.g., 18/18), number of cells in which I_{Ca} was present over the total number of cells studied; *statistically significant difference between P and VM cells data.

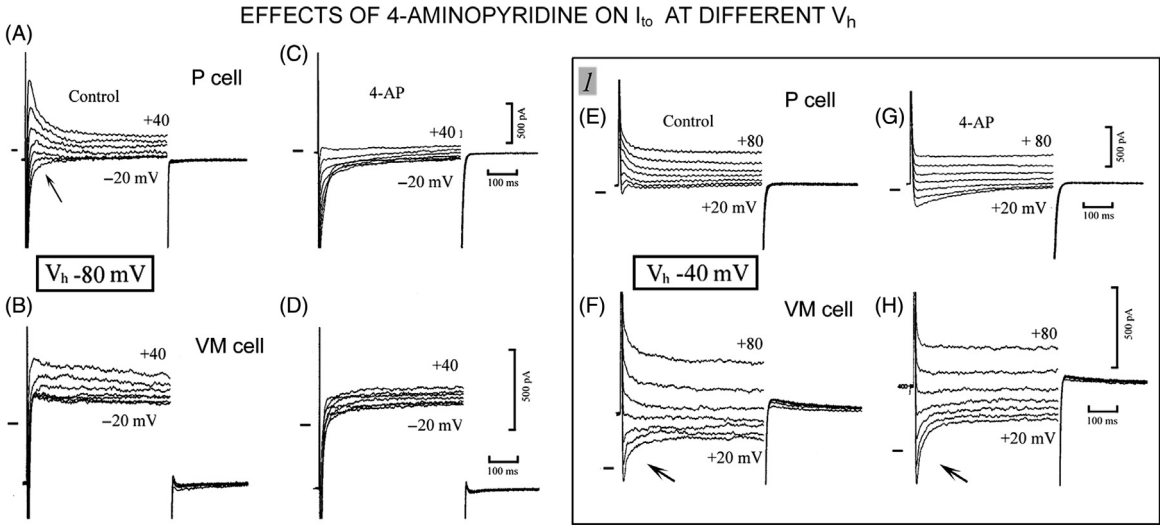

Figure 9. I_{to} in P and VM cells. In A–D, steps were applied from V_h −80 to the −20/+40 mV range. In P cell, the arrow points to slowly decaying I_{Na2} during the −20 mV step (A). The currents in a VM cell taken from a different heart are shown in B. The procedure was repeated in the presence of 4-AP in P (C) and VM cell (D). In inset 1, steps were applied from V_h −40 to +80 mV in P (E) and VM cell (F), where the arrow points to the current recorded at +20 mV. The procedure was repeated in the presence of 4-AP in P (G) and VM cell (H), where the arrow points the current recorded at +20 mV. VM cells from the same heart as in Fig. 2.

Table 11. I_{to} in VM and P cells during depolarizing steps from different V_h.

V_h to test step (mV)	Param	VM cells	P cells
−80 to +40	I_{to} (pA)	394 ± 136 (12/18)	914 ± 168* (18/18)
	τ_f (msec)	8.8 ± 1.6	13.4 ± 2.2
	τ_s (msec)	59.4 ± 9.9	147.1 ± 34.9*
	I_{to}–I_h (pA)	780 ± 189	1817 ± 248*
−70 to +40	I_{to} (pA)	235 ± 84 (10/16)	825 ± 157* (16/16)
	I_{to}–I_h (pA)	300 ± 82	1557 ± 239*
−60 to +40	I_{to} (pA)	26.7 ± 19 (2/15)	663 ± 164* (15/16)
	I_{to}–I_h (pA)	50.7 ± 34.8	1412 ± 249*
−50 to +40	I_{to} (pA)	00 ± 0 (0/16)	532 ± 88* (16/16)
	I_{to}–I_h (pA)	00 ± 0	1163 ± 177*
−40 to +40	I_{to} (pA)	00 ± 0 (0/10)	439 ± 111* (9/9)
	I_{to}–I_h (pA)	00 ± 0	948 ± 249*
−40 to +80	I_{to} (pA)	182 ± 44 (10/10)	1093 ± 220* (9/9)
	I_{to}–I_h (pA)	370 ± 52	2176 ± 327*

V_h to test step (mV), depolarizing steps from holding potential to voltage indicated; I_{to} (pA), amplitude of I_{to} in pA as the difference between I_{to} peak and the end of 500 msec steps; I_{to}–I_h (pA), amplitude of the current measured as the difference between I_{to} peak and I_h; Param, parameters measured; VM cells, data from ventricular myocardial cells; P cells, data from Purkinje cells; τ_f (msec) and τ_s (msec), fast and slow time constants, respectively, of I_{to} inactivation; Numbers in parenthesis (e.g., 18/18), number of cells in which I_{to} was present over the total number of cells studied; *statistically significant difference between P and VM cells data.

maine and Cordeiro 2007). In the P cell (Fig. 9E), the inward transients were markedly reduced and peak I_{to} was decreased. In the VM cell (Fig. 9F), inward transients were present during the +20 (arrow), +30, and +40 mV steps and I_{to} was present during the +60, +70, and +80 mV steps.

In the presence of 4-AP, in the P cell (Fig. 9G), I_{to} was eliminated and the small slowly decaying inward component was largest at 0 mV. In the VM cell (Fig. 9H), in the presence of 4-AP, I_{to} peak was eliminated and the sustained current was smaller. I_{Ca} (arrow) was largest at +30 mV and reversed between +60 and +70 mV.

Thus, I_{to} patterns were distinctly different in that in the P cell I_{to} peak was larger and declined more by the end of the step. Also, I_{to} block by 4-AP unmasked inward currents with voltage range, magnitude, and speed of inactivation consistent with I_{Na2} in P cell and with I_{Ca} in the VM cell. With V_h −40 mV, in the P cell I_{Na2} was small and in the presence of 4-AP the current decreased slowly. In the VM cell, with V_h −40 mV, I_{Ca} was larger in the presence of 4-AP and inactivated quickly.

In Table 11, with V_h −80 mV and test steps to +40 mV, in P cells I_{to} when measured as the difference between its peak and sustained current at end of 500 msec steps was larger (*) as it was when measured as the difference between I_{to} peak and I_h (*). I_{to} decreased from its peak to the end of the step by −27.1% in VM and by −45.1% in P cells, the slow time constant of inactivation being smaller in VM cells (*).

In VM cells, with V_h −70 and −60, I_{to} decreased by −40.3% and −93.2%, respectively. With V_h −50 and −40 mV there was no apparent I_{to} on depolarization to +40 mV. In P cells, with V_h −70, −60, −50, and −40 mV, at +40 mV I_{to} decreased by −9.7%, −27.4%, −41.7%, and −51.9%, respectively. With V_h −40 mV, at +80 mV (past the reversal potential of I_{Ca}) in VM cells I_{to} was smaller (*) than in P cells. The difference between peak I_{to} and I_h ($I_{to}-I_h$) was larger than I_{to} in both tissues and was much larger (*) in P cells at all V_h.

Thus, with respect to P cells, in VM cells I_{to} peak: (1) was much smaller; (2) decreased less to a smaller sustained current; (3) was reduced more or altogether eliminated by less negative V_h; and (4) could be made to reappear with steps from −40 to +80 mV, still being much smaller than in P cells.

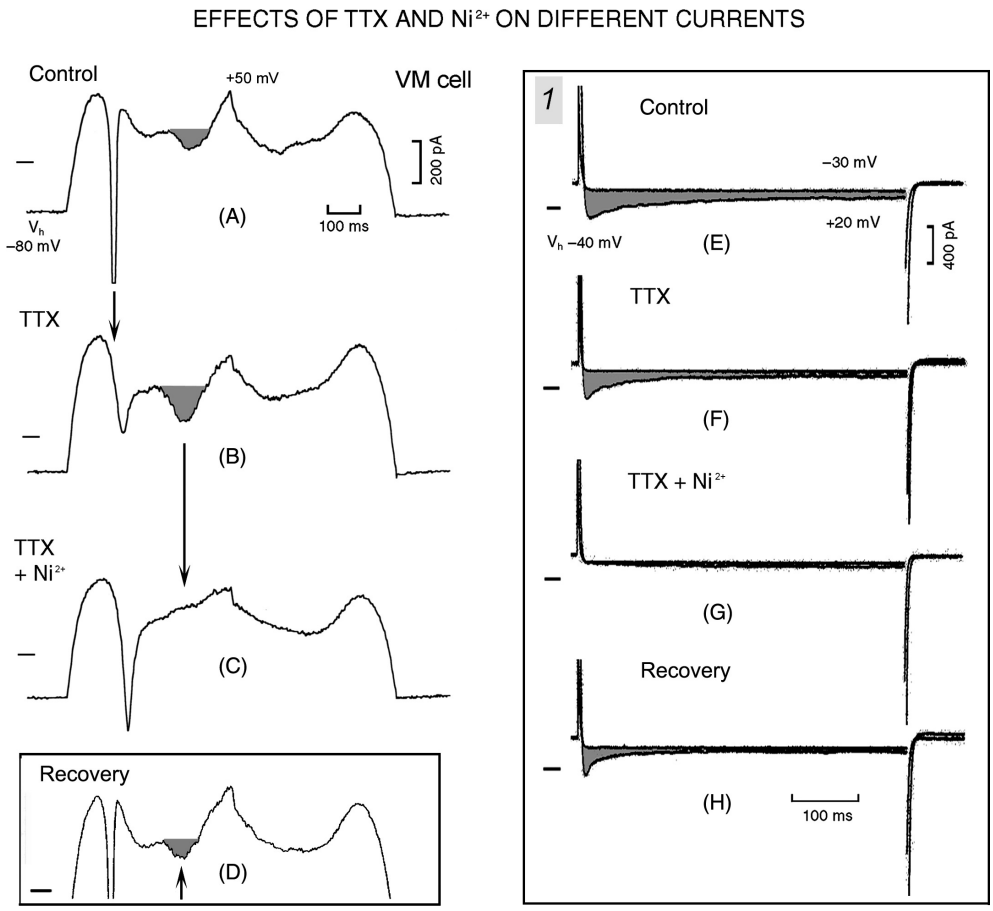

Figure 10. TTX does not eliminate I_{NS} and Ni^{2+} abolishes I_{Ca} component. In A, during the 260 mV sec^{-1} ramp, I_{Na1} was superimposed on I_{NS} which was followed by the I_{Ca} component (shaded area). TTX (30 μmol L^{-1}, B) eliminated I_{Na1} (short arrow) but not I_{NS} as confirmed by the presence of I_{PS}. Ni^{2+} (2 mmol L^{-1}, C) abolished the I_{Ca} component (long arrow). Recovery is shown in D. In inset 1, depolarizing steps from V_h −40 mV to +20 mV elicited I_{Ca} (control, E) which was not suppressed by TTX (TTX, F) but was eliminated by Ni^{2+} (TTX + Ni^{2+}, G). During the recovery from TTX and Ni^{2+}, I_{Ca} returned to control value (recovery, H).

Effect of tetrodotoxin on I_{NS} and of nickel on I_{Ca} component

In P cells, the sodium channel blocker tetrodotoxin (TTX) markedly reduces I_{NS} (Vassalle et al. 2007), including the fraction caused by I_{Na3} (Rota and Vassalle 2003). As in VM cells, sodium currents do not seem to play a dominant role in I_{NS}, TTX would not be expected to suppress the NS region. Also, if I_{Ca} is responsible for the inward component positive to I_{NS}, the Ca^{2+} channel blocker Ni^{2+} should eliminated it.

In Figure 10A, control, in the VM cell during the 260 mV sec^{-1} ramp I_{Na1} was superimposed on NS region and the I_{Ca} component was emphasized by shaded area. In Figure 10B, TTX (30 μmol L^{-1}) eliminated I_{Na1} (short downward arrow) and only I_{NS} was left. That indeed I_{NS} was not abolished by TTX is confirmed by the fact during the repolarizing ramp a distinct I_{PS} was present as in control.

In the presence of TTX, I_{Ca} (shaded area) was greater than in control. A possible reason for this increase might be that TTX decreases intracellular Na^+ activity (Abete and Vassalle 1988; Iacono and Vassalle1990), thereby increasing the transmembrane Na^+ gradient. In turn, a larger Na^+ gradient increases the extrusion of Ca^{2+} through an enhanced Na^+-Ca^{2+} exchange: this would increase the transmembrane Ca^{2+} gradient and therefore I_{Ca}.

In Figure 10C, Ni^{2+} (2 mmol L^{-1}) altogether abolished I_{Ca}, as emphasized by the long downward arrow. Although 2 mmol L^{-1} Ni^{2+} blocks also the Na^+-Ca^{2+} exchange, such a block seems unlikely to account for the observed phenomenon, as in the voltage range of I_{Ca}, the Na^+-Ca^{2+} exchange would be operating in the reverse mode generating an outward current.

During the recovery in physiological saline solution (Fig. 10D), I_{Na1} and I_{Ca} reappeared.

In another approach (Fig. 10, inset 1), depolarizing steps were applied from a V_h of −40 mV so that Na^+ channels (but not I_{Ca} channel) were inactivated. In Figure 10E, control, a step from V_h −40 mV to −30 mV did not elicit time-dependent currents, whereas depolarization to +20 mV elicited I_{Ca}. In Figure 10F, TTX (30 μmol L^{-1}) did not suppress I_{Ca} at +20 mV. In Figure 10G, adding Ni^{2+} (2 mmol L^{-1}) to TTX solution eliminated I_{Ca} and allowed a small decaying current to appear (presumably an unmasked small I_{to}). In Figure 10H, during the recovery from TTX and Ni^{2+}, I_{Ca} returned to the control value. Similar results were obtained in $n = 2$.

Effects of 4-AP and Ba^{2+} on fast and slow ramps in myocardial cells

In Purkinje cells, Cs^+ and Ba^{2+} (blockers of I_{K1}) markedly decreased I_{K1} as well as the slope conductance, but only slightly reduced the outward current at positive potentials (Du and Vassalle 1999). Furthermore, Ba^{2+} eliminated I_{K1} peak but not I_{NS}, whereas low V_h and TTX eliminated I_{NS} (Rota and Vassalle 2003; Vassalle et al. 2007). As neither a low V_h nor TTX abolished I_{NS} in VM cells (present results), in VM cells I_{NS} might be mostly related to Mg^{2+}

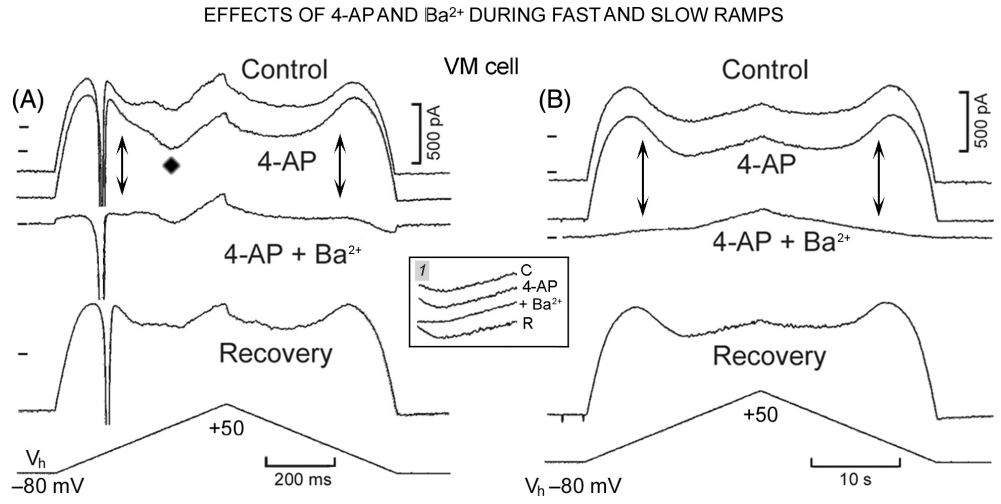

Figure 11. NS and PS regions are abolished by Ba^{2+}. In A, 260 mV sec^{-1} ramps were applied in control, in the presence of 4-AP, of 4-AP plus Ba^{2+}, and during recovery. In B, the same procedures were applied during 6.5 mV sec^{-1} ramp. The larger I_{Ca} component in the presence of 4-AP is labeled with a rhombus. In the two panels, the left hand double headed arrows emphasize the disappearance of I_{NS} and the right hand double headed arrows that of I_{PS}. In inset 1, the current traces recorded between I_{Ca} and ramp peaks in B have been superimposed: C, control; 4-AP, in the presence of 4-aminopyridine; +Ba^{2+}, in the presence of 4−AP and Ba^{2+}; R, recovery in physiological saline solution.

block of I_{K1}. To verify this point, in one experiment fast and slow ramps were applied to test whether Ba^{2+} (by blocking I_{K1} and therefore preventing the block and unblock by Mg^{2+} in the NS and PS regions, respectively) abolished I_{NS} and I_{PS}.

In Figure 11A, in a VM cell, during a 260 mV sec^{-1} ramp (bottom trace), in control the current exhibited the usual features. In the presence of 4-AP, I_{NS} was little changed whereas I_{Ca} component became larger (+129%, rhombus). While overall the current was less outward, I_{K1} and I_{PS} peaks were somewhat larger. The current between I_{Ca} and ramp peaks was unchanged (+1.6%) as in P cells (Du and Vassalle 1999). In the presence of Ba^{2+}, not only the I_{K1} peak, but also I_{NS} and I_{PS} were abolished (as pointed out by double headed arrows). Neither the outward current between I_{Ca} and ramp peaks nor the initial fast decrease in current at beginning of repolarization was suppressed. I_{NS} and I_{PS} reappeared during recovery (bottom current trace).

In Figure 11B, during a 6.5 mV sec^{-1} ramp (bottom trace), in the presence of 4-AP, I_{K1} peak was also somewhat larger and so was I_{Ca}. Instead, the current between I_{Ca} and ramp peaks was not affected (−0.6%, see 4-AP trace in Figure 11 inset 1). Ba^{2+} abolished I_{K1} peak and I_{NS}, as pointed out by the left hand double headed arrow, leaving only the slowly increasing outward current. As in P cells (Du and Vassalle 1999), the current during the last part of the depolarizing ramp was unaffected (see Ba^{2+} trace in Figure 11 inset 1). During the repolarizing ramp, the current decreased continuously (no I_{PS}, as indicated by the right hand double headed arrow). The recovery from the procedures is shown by the bottom current trace and by trace R in Figure 11 inset 1).

Thus, while in P cells Ba^{2+} abolished I_{K1} peak, but not I_{NS} (Rota and Vassalle 2003), in VM cells it abolished I_{K1} peak, I_{NS} and I_{PS}. However, neither 4-AP nor Ba^{2+} abolished the increase in outward current between I_{Ca} and ramp peaks.

Discussion

The present results show numerous dissimilarities between VM and P cell currents. The features involved concern: (1) the slope conductance at the resting potential and its changes during depolarization and repolarization; (2) the sodium currents I_{Na1}, I_{Na2}, and I_{Na3} (presence or absence, amplitude, threshold, voltage and time dependence, contributions to peak sodium current); (3) outward and inward current during ramps with different slopes; (4) time and voltage dependence of I_{K1} blocking and unblocking; (5) NS and PS regions (voltage range, voltage and time dependence, slope conductance, depolarization vs. repolarization); (6) prevalent role of slowly inactivating sodium currents in the mechanisms underlying NS region in P cells; (7) prevalence of block and unblock of I_{K1} in NS and PS regions, respectively, in VM cells; (8) characteristics of I_{Ca} as well as I_{to} and sustained current; (9) different contributions of I_{K1} and I_{to} to the I-V relation; (10) voltage and time dependence of currents during repolarizing ramps, and (11) response to channels blockers.

We conclude that the differences between VM and P cells involved all the ionic currents studied and account for several electrophysiological differences in resting and action potentials.

Membrane conductance as a function of voltage and time in VM and P cells

As at negative potentials I_{K1} predominates in determining the I-V relation (Shah et al. 1987), at potentials negative to I_{K1} peak the I-V relation was taken to essentially reflect that of I_{K1}. Near the resting potential, the larger slope conductance in VM cells (+100%) is consistent with the findings that I_{K1} in rabbit myocardial ventricular cells is larger than in P cells (Cordeiro et al. 1998). Indeed, the expression of transcripts underlying I_{K1} channel (Kir2.1, Kir2.2, Kir2.3) in human Purkinje fibers is about half that in ventricular myocardium (Gaborit et al. 2007).

The larger slope conductance in VM cells at resting potential could be related to the fact that I_{K1} channels are located also in T-tubules (e.g., Lopatin and Nichols 2001), which are absent in P cells (see Vassalle et al. 1995 for references). In VM cells, the larger I_{K1} peak could possibly be due to the larger resting conductance and/or to lower polyamines level in myocardial cells.

The smaller conductance in P cells would seem at odds with the fact that in 2.7 mmol L^{-1} $[K^+]_o$ their maximum diastolic potential (~−95 mV; e.g., Vassalle 1965) is more negative than the resting potential in VM cells (~−80 mV). This discrepancy is due to the presence of the pacemaker current I_{Kdd}, (the potassium current underlying diastolic depolarization; Vassalle 1966; Vassalle et al. 1995; Vassalle 2007, 2013), which is present in P cells, but not in VM cells.

Thus, in quiescent P cells in 5.4 mmol L^{-1} $[K^+]_o$ the *resting* potential is ~−80 mV and does not increase when $[K^+]_o$ is lowered to 2.7 mmol L^{-1} (Vassalle 1965, 1966) due to K^+-dependent fall in K_1 channel conductance. However, in cells active in 2.7 mmol L^{-1} $[K^+]_o$, the activation of I_{Kdd} during the AP (Vassalle 1966; Vassalle et al. 1995) is responsible for the voltage undershoot to the maximum diastolic potential. As I_{Kdd} deactivates as a function of time in the diastolic potential range, the pacemaker potential and slope conductance decrease toward the resting potential value (Weidmann 1951; Vassalle

1965, 1966). Therefore, in P cells diastolic conductance at *resting* potential is mostly a function of I_{K1} (as in VM cells) and at the *maximum diastolic potential* of both I_{K1} and I_{Kdd}.

During ramp depolarization, the progressive decline of slope conductance to a minimum at I_{K1} peak shows that the gradually smaller increase in outward current is due to I_{K1} inward rectification, rather than a progressive increase of an inward current. At I_{K1} peak, I_{K1} is matched by the inward current, as the outward current stopped increasing and the slope conductance became minimal (Fig. 6). Soon after, in both tissues, the activation of I_{Na3} (together with the decreasing I_{K1}) accounts for the initiation of the NS region.

During I_{NS}, the reversal and reincrease of pulse current indicate that I_{K1} became smaller than the inward current. In fact, I_{K1} reaches its minimum at the peak of I_{NS} (−20 mV in P cells) as shown by I_{K1} I-V relation (control minus I_{K1} blockers) (Shah et al. 1987; Cordeiro et al. 1998). In P cells, the reversal of pulse current occurred both during the part of I_{NS} due to I_{Na3} (Rota and Vassalle 2003) and that due to the inactivation of I_{Na2} (Bocchi and Vassalle 2008). The relation of the reversed pulse current to the activation and decay of I_{Na2} is demonstrated by the findings that during depolarizing steps the amplitude of pulse current became larger when I_{Na2} appeared, decreased gradually during I_{Na2} slow inactivation, and was markedly reduced by lidocaine (Bocchi and Vassalle 2008).

However, as pulse current reversal in NS range occurred also during the 6.5 mV sec^{-1} ramp (Fig. 6E) when the Na^+ currents are inactivated (and in VM cells the inactivating I_{Na2} would play little role), the reversal appears to involve also the block of I_{K1} channel. In both cases (increase in Na^+ currents and decrease in I_{K1}) the net current would become inward (I_{NS}) and therefore the pulse current would reverse. The role of I_{K1} change in pulse current reversal is supported by the occurrence of the reversal also during I_{PS} (Fig. 6D and E), when any possible residual Na^+ currents would be inactivated.

Contribution of I_{Na3}, I_{Na2}, and rectification of I_{K1} to NS region in P and VM cells

Our findings show that the mechanisms underlying I_{NS} in P cells differ qualitatively and quantitatively from those in VM cells and account for some previously reported results.

In the presence of TTX and of Ca^{2+} blocker nicardipine in rabbit, the NS region was present in VM cells but not in P cells (Cordeiro et al. 1998). This difference is accounted by the finding that I_{Na3} (Rota and Vassalle 2003) and I_{Na2} (Vassalle et al. 2007; Bocchi and Vassalle 2008) are blocked by TTX. However, when measured as the difference current (control minus Ba^{2+}), a small NS region was present also in P cells (Cordeiro et al. 1998), suggesting that, in the absence of Na^+ and Ca^{2+} currents, the residual I_{NS} was due to a block of I_{K1}.

Similarly, in P cells with steps from a V_h of −50 mV, the NS region was not always found, but it was present in I_{K1} I-V relation (control minus current in Ba^{2+} or Cs^+) (Shah et al. 1987). In retrospect, at V_h −50 mV the Na^+ currents would have been inactivated or markedly reduced (Rota and Vassalle 2003; Vassalle et al. 2007; present results). Therefore, the findings of Shah et al. (1987) can also be accounted for by the inactivation of Na^+ currents at −50 mV and a small contribution of I_{K1} block to I_{NS} in P cells. That in P cells, I_{K1} rectification contributes to I_{NS} is also indicated by a net decrease of radioactive K^+ efflux in the −60 to −40 mV range (e.g., Vereecke et al. 1980).

In our experiments, in the absence of blockers, with respect to VM cells, in P cells the increase in I_{NS} with the steeper ramps and its decrease or absence with 6.5 mV sec^{-1} ramp are consistent with time-dependent inactivation of I_{Na3} and I_{Na2}. In P cells, with V_h −80 mV, the smaller I_{NS} in I-V relation of the sustained current is consistent with inactivated I_{Na3} and substantially reduced I_{Na2} by the end of 500 msec steps. In addition, the gradual decrease of I_{NS} with less negative V_h in P but not in VM cells (Fig. 4, inset 1) indicates a voltage-dependent inactivation of Na^+ currents.

Conversely, with 6.5 mV sec^{-1} ramps the much smaller I_{NS} in P cells is explained by I_{Na3} and I_{Na2} being reduced or absent, in agreement with the little effects of TTX on I_{NS} and by the similar values of I_{NS} and I_{PS}. Furthermore, with V_h −50 mV, during fast ramps the near abolition of I_{NS} in P cells but not in VM cells also points to a greater role of Na^+ currents.

In P cells, TTX, lidocaine, and low V_h markedly reduced I_{Na3} (Rota and Vassalle 2003) as well as I_{Na2} (Vassalle et al. 2007) and so did low $[Na^+]_o$ (Bocchi and Vassalle 2008). Yet, I_{NS} persisted in VM cells with some of these procedures (present results). Furthermore, in P cells, Ba^{2+} abolished I_{K1} peak but not I_{NS} (Rota and Vassalle 2003) whereas it abolished I_{K1} peak, I_{NS}, and I_{PS} in VM cells.

These results indicate a predominant role of Na^+ currents in P cell I_{NS} and of I_{K1} inward rectification in VM cell I_{NS}. Indeed, in guinea pig ventricular myocytes, the K^+ channel opener cromakalim abolished I_{NS} and markedly shortened the action potential (Liu et al. 1990).

As for voltage ranges of Na^+ currents and of I_{NS}, the beginning of I_{NS} during the ramps (~−58 mV) indicates the participation of I_{Na3} as in P cells this current started at ~−58 mV (Table 8; Rota and Vassalle 2003) and peaked before or by the end of ramps to −42 mV (Rota and Vassalle 2003). In both P and VM cells, I_{Na3} contrib-

uted to I_{NS} prior to I_{Na1}, but (its slow inactivation being cut off by I_{Na1}) presumably little after I_{Na1}.

In P cells, the slowly inactivating I_{Na2} can contribute to I_{NS} after the inactivation of I_{Na1}, as I_{Na2} has a −40 mV threshold and is largest at a voltage (−30/−20 mV, Vassalle et al. 2007) which is near to the peak of I_{NS} (−26.5 mV with 260 mV sec^{-1} ramp). I_{Na2} activates also in the absence of I_{Na1} (Fig. 5B and E), in agreement with the findings of Bocchi and Vassalle (2008). Indeed, in those P cells in which I_{Na1} was not present with 260 mV sec^{-1} ramps, I_{NS} peaked at a potential (−29.2 mV, present results) near the I_{Na2} peak.

Therefore, with respect to VM cells, in P cells I_{NS}: (1) had a smaller voltage range; (2) was larger with faster ramps; and (3) was smaller with slow ramps, with lower V_h and in the presence of TTX. These finding indicate a predominant role of the sodium currents in I_{NS} of P cells and of I_{K1} block in VM cells.

Dual mechanism of I_{K1} inward rectification and the NS and PS regions in P and VM cells

As for the inward rectification of I_{K1} channel, two mechanisms have been demonstrated: block by intracellular polyamines (channel gating by spermine and spermidine; Lopatin et al. 1994; see Lopatin and Nichols 2001) and block by Mg^{2+} (Matsuda et al. 1987; Vandenberg 1987). The I_{K1} block by spermine and spermidine is time dependent (Ishihara 1997), whereas the block by Mg^{2+} and putrescine is voltage dependent and virtually instantaneous (Ishihara and Ehara 1998).

In guinea pig VM cells, in the absence of internal Mg^{2+}, the block by polyamines occurs between −80 and ~−40 mV whereas, with in the presence of internal Mg^{2+}, I_{K1} block is present also between −40 and 0 mV (Ishihara 1997). Furthermore, after a depolarization larger than 0 mV (which would cause Mg^{2+} block), on repolarization to −50 mV there was a sudden transient increase in outward current (see also Shimoni et al. 1992). The amplitude of the outward current was correlated to the degree of Mg^{2+} block during the previous depolarization, indicating that the increase in outward current was due to the removal of Mg^{2+} block. During a repolarizing ramp, the outward current at −50 mV was substantially larger in the presence than in the absence of internal Mg^{2+}, indicating the importance of the removal of Mg^{2+} block of I_{K1} for the repolarization of the action potential (Ishihara 1997; Ishihara and Ehara 1998).

Because I_{K1} block by polyamines begins at more negative voltage than that by Mg^{2+} (Ishihara et al. 1989; Ishihara 1997; Ishihara and Ehara 1998), the block of I_{K1} ought to be solely due to polyamines up to I_{K1} peak which with the slowest ramp occurred at −44.2 mV in VM cells (Table 5). Instead, the voltage range of the I_{K1} block by Mg^{2+} (−40 to 0 mV) overlaps the NS region in VM cells.

Time dependence of I_{K1} block by polyamines at the beginning of depolarizing steps would account for the initial decline of the outward current. On step repolarization from positive potentials toward E_K the sudden increase in outward current due to instantaneous relief of Mg^{2+} block gradually declined due to time-dependent block by spermine and spermidine (Ishihara 1997). The time constant of the exponential decay of the outward current was ~5 msec at −50 mV which is close to the τ of ~6 msec for the current decline on depolarization from V_h −80 to ~−60 mV (Table 4).

As for the symmetrical voltage ranges of NS and PS regions, if the voltage-dependent block of I_{K1} by Mg^{2+} initiates near the beginning of I_{NS}, its complete removal at the peak of I_{PS} (*ceteris paribus*) should occur at a similar potential. Indeed, in VM cells, with the slowest ramp, I_{NS} initiated at −44.2 mV and I_{PS} peaked at −44.4 mV and their amplitudes were similar (218 and 197 nA, respectively). The peak of I_{NS} (full block) was at −3.9 mV and the beginning of I_{PS} was 8.9 mV (initiation of block removal) (Table 5).

With faster ramps, other factors modified I_{K1} and I_{PS} peaks. In P cells, the larger I_{NS} with faster ramps implicates additional time-dependent factors such as a greater activation of I_{Na3} and of I_{Na2}. In keeping with this conclusion, in P cells with 6.5 mV sec^{-1} ramp, I_{NS} was much smaller and so was I_{PS}, as the Na^+ currents would be inactivated during the depolarizing and repolarizing ramp.

That I_{K1} undergoes a progressively greater inward rectification on depolarization from the V_h is also shown by the progressively smaller increase in sustained outward current at the end of 500 msec depolarizing steps (when most of the other currents would be completely or partially inactivated). Actual decline of the sustained current at potentials positive to −50 mV in P and to −40 mV on VM cells reflects the I_{NS} seen during the ramps. The less negative potential at which the sustained current decreased with respect to the beginning of I_{NS} during the ramps might be ascribed to lack of I_{Na3} contribution to the sustained current.

At more negative potentials, block and unblock of I_{K1} might contribute to several changes in the I-V relation during ramps of different steepness. Thus, voltage- and time-dependent block by spermine and spermidine on depolarization from V_h −80 mV to I_{K1} peak would account for the gradually smaller increase of outward current during a ramp and for the decreasing slope conductance both in P (Rota and Vassalle 2003; Bocchi and Vassalle 2008; present results) and in VM cells (Fig. 6).

As at less negative potentials the channel block by polyamines is much slower (Ishihara et al. 1989; Ishihara and

Ehara 1998), such a block may also contribute to the current changes that occur during the ramps with steeper slopes. A greater lag between faster voltage change and block of I_{K1} channel might be responsible for the increase in magnitude of I_{K1} peak with faster ramps. Also, the larger decrease in outward current during faster repolarizations might include a delay in the removal of I_{K1} block by polyamines.

The fact that during repolarizing 260 mV sec^{-1} ramps, in P cells I_{PS} was much smaller (−81%) than I_{NS} (Table 6) suggests that I_{Na3} and I_{Na2} have a major role in I_{NS} and that the remainder (~19%) is due to I_{K1} block by Mg^{2+}. The removal of I_{K1} block would account for the I_{PS} beginning being more outward (no Na^+ currents contribution) than the I_{NS} peak and I_{PS} peak being similar to I_{NS} beginning. In contrast, in VM cells the similarity of I_{NS} and I_{PS} (Table 6) suggests that block and unblock of I_{K1} channel by Mg^{2+} were the major mechanisms underlying I_{NS} and I_{PS}, respectively.

This is consistent with Mg^{2+} block and unblock being only voltage dependent and with the slowly inactivating I_{Na2} not contributing to either I_{NS} or I_{PS} in VM cells. During the slowest ramps, there would be little or no contribution by Na^+ currents to either I_{NS} or I_{PS}, as supported by the similarity of I_{NS} and I_{PS} in VM as well as in P cells (Table 5).

In VM cells, with 260 mV sec^{-1} ramp the larger difference between I_{PS} peak and I_h (Table 6) reflected the almost double I_{K1} upon which I_{PS} was superimposed. In contrast, the similarity of the I_{PS} peak voltage in VM and in P cells is consistent with the voltage dependence of the removal of I_{K1} block by Mg^{2+}. With the 6.5 mV sec^{-1} ramp, the much larger I_{NS} and I_{PS} in VM than in P cells support the role of Mg^{2+} block and unblock, respectively, as in both tissues the Na^+ currents would be largely inactivated during both depolarizing and repolarizing ramps.

Therefore, the time- and voltage-dependent block of I_{K1} by polyamines appears to prevail at potentials negative to the I_{K1} peak whereas the inward rectification of I_{K1} during I_{NS} is attributable to Mg^{2+} block. This conclusion is supported by the findings that in P cells: (1) when I_{Na3} and I_{Na2} were present, I_{NS} was larger than in VM cells and more so the faster the ramp; (2) when I_{Na3} and I_{Na2} were inactivated (repolarizing ramps) I_{PS} was smaller in P cells; and (3) with the slowest ramp (I_{Na3} and I_{Na2} being inactivated during the depolarizing and repolarizing phases), both I_{NS} and I_{PS} were smaller in P cells.

I_{Na3} in Purkinje and myocardial cells

With the approach of Rota and Vassalle (2003), in P cells I_{Na3} was mostly studied at potentials negative to I_{Na1} threshold. With depolarizing ramps (in the absence of I_{Na1}), I_{NS} began at −57.7 mV and peaked before or by the end of the ramp at −42 mV. I_{NS} was attributed to the activation of I_{Na3}, as shown by its threshold, the marked reduction by TTX and lidocaine and its little sensitivity of Cs^+ and Ba^{2+}. In contrast to I_{Na3}, TTX or lidocaine did not abolish I_{CaT} (Tytgat et al. 1990). In addition, I_{Na3} was markedly reduced by 70 mmol L^{-1} $[Na^+]_o$ and it was not abolished by 100 μmol L^{-1} Ni^{2+} (M. Rota and M. Vassalle, unpubl. experiments). These findings contribute to rule out that I_{Na3} might in actuality be I_{CaT}.

Suitably large and slow ramps that did not activate I_{Na1} initiated I_{Na3} at about −60 mV followed at about −40 mV by the activation of I_{Na2} (Rota and Vassalle 2003). In retrospect, these results in P cells separated for the first time the contributions of I_{Na3} and I_{Na2} to I_{NS}. That I_{Na3} is a sodium current also in VM cells is shown by its decrease with less negative V_h (depolarizing steps, Table 1) or ramps (Table 9).

A population of slowly inactivating Na^+ channels has been also reported in giant squid action. These channels are much fewer than the normal Na^+ channels, activate on depolarization to ~−65 mV whereas I_{Na} threshold is −50 mV, activate maximally at −40 mV and undergo a very slow inactivation (Gilly and Armstrong 1984), similar to I_{Na3}. As for the mechanism by which I_{Na1} block I_{Na3} slow inactivation, it appears that fast I_{Na1} inactivation blocks slow inactivation of Na^+ channels by charge immobilization (Richmond et al. 1998).

As to Na^+ channel isoforms involved in I_{Na3}, among several Na^+ channels isoforms cloned (Na_V1 to Na_V9; cardiac, neuronal, and skeletal), cardiac $Na_V1.5$ isoform has a low TTX-sensitivity, whereas the neuronal ($Na_V1.1$, $Na_V1.2$, $Na_V1.3$, $Na_V1.6$) and skeletal muscle ($Na_V1.4$) isoforms have a high TTX-sensitivity (Zimmer et al. 2002; Haufe et al. 2005a). The neuronal $Na_v1.2$, $Na_v1.3$, and $Na_v1.6$ isoforms are expressed in VM cells and $Na_v1.1$ and $Na_v1.2$ (Haufe et al. 2005a) as well as skeletal $N_{aV}1.4$ isoform (Qu et al. 2007) have been identified in P cells. Although I_{Na3} and I_{Na2} are more sensitive to TTX block than I_{Na1}, the noncardiac channels isoform involved is not known, as the skeletal muscle Na^+ channel isoform $Na_v1.4$ expressed in P cells is also blocked by low concentrations of TTX (Qu et al. 2007).

The neuronal TTX-sensitive Na^+ channels were found to contribute to peak sodium current by 22% in P cells and by 10% in VM cells (Haufe et al. 2005*b*) and therefore to the sodium current responsible for the AP upstroke. Our results show that at the I_{Na1} threshold, I_{Na3} was a sizeable fraction of the total I_{Na} current. However, because I_{Na1} was truncated by the saturation of the amplifier consistently in P cells and often in VM, the I_{Na3} contribution to the total I_{Na} is bound to be overestimated. In

addition (as shown by means of double steps), the fast inward component of I_{Na2} would be expected to contribute to the total Na^+ influx during the upstroke.

I_{Na3} appears to be the link between DD and upstroke of AP in P cells by being responsible (Rota and Vassalle 2003) for the depolarizing phase of ThV_{os} (the oscillatory potentials near the threshold for the upstroke; Vassalle 1965; Spiegler and Vassalle 1995; Berg and Vassalle 2000). Successive ThV_{os} increase progressively in size during diastole until the depolarizing phase becomes large enough to attain the threshold for I_{Na1} (Vassalle 1965; Spiegler and Vassalle 1995; Berg and Vassalle 2000). In P fibers, TTX suppressed the spontaneous discharge by abolishing the upward swing of the late diastolic depolarization, although the fibers could still be electrically driven due to smaller sensitivity of I_{Na1} to TTX (see Fig. 3 by Vassalle and Scidà shown in Vassalle 1980). ThV_{os} are present also in sino-atrial node (Kim et al. 1997) and are essential for both the initiation and maintenance of spontaneous activity of cardiac pacemakers (Vassalle 2007, 2013).

In VM cells, the voltage gap between the resting potential and the threshold for I_{Na3} is closed by the depolarization induced by the conducted AP, as of necessity I_{Na3} threshold is less negative than the resting potential. I_{Na3} would then speed up the attainment of I_{Na1} threshold and the induction of the upstroke.

While a 5 mmol L^{-1} $[Na^+]_o$ has been successfully used to compare Na^+ currents in normal and diseased VM cells (Pu and Boyden 1997; Valdivia et al. 2005), the low $[Na^+]_o$ solution markedly reduced I_{Na1}. This apparently makes it unsuited to study the much smaller I_{Na3}, as no slowly inactivating I_{Na3} was apparent in those studies. In our experiments, I_{Na3} was demonstrated under physiological conditions at potentials negative to I_{Na1} threshold. Also, less negative V_h markedly reduced I_{Na1} (Table 2) leaving a separately identifiable slowly inactivating I_{Na3} (Table 1).

Thus, the present results show that I_{Na3}: (1) was also present in VM cells; (2) had threshold that was negative to that of I_{Na1} and was less negative than that in P cells; (3) inactivated slowly; (4) could occur at potentials less negative than I_{Na1} threshold (as shown by preventing I_{Na1} activation); (5) was less inactivated at a lower V_h than I_{Na1}; (6) increased in amplitude during depolarizing steps past ~−60 mV due to its voltage-dependent activation and during faster depolarizing ramps (greater Na^+ channel availability); (7) contributed to magnitude of total Na^+ influx associated with I_{Na1}; (8) was absent during repolarizing ramps; (9) was associated with a reversal of pulse currents and with an increase in slope conductance during I_{NS}; and (10) its slow inactivation was suppressed by I_{Na1}.

A limitation of our study is represented by the lack of measurements of membrane capacitance (Cm) in the two cell populations analyzed, posing concerns related to the comparison of ionic current amplitudes. In this regard, values of Cm of 121.9 ± 4.8 pF (Rota and Vassalle 2003) and of 125 ± 6 pF (Han et al. 2000) have been reported for canine P cells, whereas Cm values of 113 ± 6 pF (Han et al. 2000) and of 133.4 ± 6 pF (Pu and Boyden 1997) have been reported for canine VM cells. Thus, the average value of the above capacitances for the P cells is 123.4 pF and that for the VM cells is 123.2 pF.

While P cells have no T tubule system, which is present in VM cells, P cells are larger in size than VM cells. Thus, these two features (cell size and T tubule system) tend to offset each other in determining the surface area in the cell populations.

The fast sodium current I_{Na1} in P and VM cells

The measurement of I_{Na1} magnitude in P and VM cells was hindered by its being truncated by the saturation of the amplifier. However, the finding that with V_h −80 mV I_{Na1} was consistently cut off at −10 nA in P cells but only in 13/18 in VM cells indicates that I_{Na1} was smaller in VM than in P cells. Furthermore, with less negative V_h (Na^+ channels being partially inactivated), I_{Na1} was less often truncated and yet in VM cells I_{Na1} was still smaller than in P cells. Also, the less frequent I_{Na1} activation during the 260 mV sec^{-1} ramp in P cells suggests that during this slower ramp I_{Na1} channels are more susceptible to time-dependent inactivation in P than in VM cells.

Several differences regarding I_{Na1} in P and VM cells have been reported. Thus, total amplitude and maximal rate of rise of AP upstroke were much larger in Purkinje than in ventricular fibers (Baláti et al. 1998). Also, neuronal sodium channels contribute less to the peak sodium current in dog ventricular than in Purkinje fibers (Haufe et al. 2005b). A larger I_{Na1} with a more negative threshold in P cells (present results) would contribute to the faster conduction of P cells with respect to VM cells. Both in nonspontaneous P and VM cells, conducted action potentials would depolarize the membrane to the threshold of I_{Na3}, which in turn would allow the attainment of I_{Na1} threshold, as seen during the ramps.

The slowly inactivating I_{Na2}

In VM cells, the absence of a large slowly decaying component of I_{Na2} comparable to that of P cells accounts for the fact that (see Introduction), in contrast to P cells, the AP duration of ventricular myocytes was very little affected by TTX, local anesthetics, veratridine, and high

$[Na^+]_o$, suggesting that there is little or no slow decaying I_{Na2} in VM cells under physiological conditions. I_{Na2} is more sensitive to TTX than I_{Na1} (Vassalle et al. 2007) and therefore is possibly due to the activation of neuronal or skeletal muscle isoforms. In P cells, the larger contribution of the noncardiac Na^+ channels (Haufe et al. 2005b) might be due to both I_{Na3} and I_{Na2}. In P cells, the fast activation of I_{Na2} (Bocchi and Vassalle 2008) would contribute to the influx of Na^+ during the upstroke and its slow inactivation contributes to the longer plateau.

A late I_{Na} was found in canine myocardial cells perfused in a K^+-free and very low Cl^- medium by applying a 2000-msec pulse to −130 mV (to remove steady-state inactivation) prior to depolarizing steps applied at intervals of 30 sec (Zygmunt et al. 2001). Our results show that I_{Na2} is small or absent under physiological conditions in VM cells, in contrast to P cells.

However, the findings of Zygmunt et al. (2001) could suggest that under abnormal situations remodeling may shift the voltage range of the late I_{Na} activation to less negative values. In this regard, it is of interest that I_{NaL} was increased in cardiac failure and yet no differences were found in isoform NaV1.1, 1.3, 1.5 subunits and in the subunit b1 and b2, leading to the conclusion that I_{NaL} increase was not due to a subunit isoform switching or to an altered b subunit expression (Valdivia et al. 2005).

In normal human ventricular myocytes, there is little or no I_{Na2} but in myocytes from patient with hypertrophic cardiomyopathy remodeling leads to the appearance of a late Na^+ current. Ranolazine, a blocker of the late Na^+ current, had negligible effect on the action potential duration of normal ventricular myocytes, but shortened the longer AP of the myopathic myocytes and reduced the related arrhythmias (Coppini et al. 2013). Therefore, under some pathological conditions remodeling-related I_{Na2} may induce arrhythmias also in VM cells.

As for role of P cell slowly inactivating I_{Na2} in cardiac arrhythmias, an increase in I_{Na2} (but not of I_{Na1}) by neurotoxins anthopleurin or ATX II in Purkinje fibers led to the onset of Torsades de pointes. This electrophysiological mechanism appears responsible for congenital and acquired long QT syndromes (LQTS), as abnormally prolonged repolarizing phase of AP leads to early afterdepolarizations (EADs) in Purkinje fibers. In vitro and in vivo, in Purkinje fibers the neurotoxins induced EADs were abolished by concentrations of mexiletene that had little effect on I_{Na1} (El-Sherif and Turitto 2003). The present characterization of differences between P and VM cells add insights relevant to mechanisms underlying some LQTS syndromes, especially the drug-induced acquired syndromes.

The calcium current in P and VM cells

That I_{Ca} was larger in VM cells was shown by the appearance of a large inward component, which peaked in the +10 to +20 mV range and became more conspicuous after the block of I_{to} by 4-AP. Instead, in P cells, the smaller I_{Ca} appeared as an indentation on I_{to} trace or it was not altogether apparent, even in the presence of I_{to} block by 4-AP.

That the inward component peaking at positive values was due to I_{Ca} was shown by its persistence at low V_h and by the abolition by Ni^{2+} of both the inward component during the ramps and I_{Ca} during depolarizing steps. In VM cells, I_{Ca}-induced positive shift of the onset of the smaller outward current would contribute to the more positive plateau and the larger I_{Ca} to the greater force of contraction (Lin and Vassalle 1978) with respect to P cells.

As for the identity of Ca^{2+} currents, the L-type (I_{CaL}, isoform $Ca_v1.2$ containing the pore forming α1C subunit) and T-type (I_{CaT}, isoforms $Ca_v3.1$, $Ca_v3.2$, and $Ca_v3.3$) are expressed both in P and M cells, I_{CaT} being more abundantly expressed in P cells and I_{CaL} predominating in VM cells (see Dun and Boyden 2008). These differences suggest that calcium current recorded in VM cells is of the I_{CaL} type, in accordance with fact that it was recorded with less negative V_h and at less negative voltage.

The transient outward current I_{to} in P and VM cells

With respect to VM cells, in P cells a larger I_{to} contributed to the much larger outward current between I_{NS} and ramp peaks, consistent with the shift of the plateau to more positive values by 4-AP (Kenyon and Gibbons 1979; Dumaine and Cordeiro 2007).

However, our results show that the *total* outward current included different components in P and VM cells, as in VM cells a smaller I_{to} was superimposed on a larger I_{K1}. In VM cells, the smaller I_{to} would induce a smaller phase 1 repolarization and (together with the larger I_{Ca}) would contribute to the more positive plateau than in P cells (e.g., see Fig. 1 in Baláti et al. 1998).

The finding that 4-AP abolished the peak I_{to}, but only reduced the sustained current at the end of depolarizing steps and the outward current during latter part of depolarizing ramps agrees with the results shown in other reports (no elimination of sustained current by 4-AP; Kenyon and Gibbons 1979; Cordeiro et al. 1998; Han et al. 2000). Therefore, I_{to} may have a time-independent background component or it may not inactivate completely (Kenyon and Gibbons 1979).

Also, there might be the contribution of an unidentified outward current present at positive potentials which is not eliminated by 0 mmol L^{-1} $[K^+]_o$ (Ishihara et al. 1989). Even I_{K1} block by Cs^+ and by Ba^{2+} did not suppress the increase in outward current at potentials positive to −40 mV, as shown by figures in Shah et al. (1987) and reported by Du and Vassalle (1999). This is consistent with the finding that ^{42}K efflux at potential positive to −30 mV was not blocked by Cs^+ (Vereecke et al. 1980).

This could be due either to the voltage dependence of Cs^+ induced block as it is for Ba^{2+} (Hirano and Hiraoka 1986) or to a Cs^+ insensitive outward rectifier. In the experiments of Cordeiro et al. (1998), 0.1 mmol L^{-1} Ba^{2+} reduced the inward I_{K1}, but did not decrease the large outward current at positive potentials. In P cells (Du and Vassalle 1999) and in VM cells, 2 mmol L^{-1} Ba^{2+} eliminated I_{K1} peak, but did not eliminate the outward current at positive potentials.

However, this *per se* does not rule out a contribution of I_{K1} to the outward current, as Ba^{2+} block of I_{K1} is removed on depolarization and slowly reestablished on repolarization (Hirano and Hiraoka 1986; Imoto et al. 1987; Valenzuela and Vassalle 1991). Therefore, in P cells after I_{NS} peak, the increase in outward current includes I_{to} (which is not blocked by Ba^{2+}, e.g., Cordeiro et al. 1998; Du and Vassalle 1999) and a current which is not suppressed by 4-AP, Ba^{2+}, Cs^+, or 0 mmol L^{-1} $[K^+]_o$. The delayed rectifier I_K could contribute to the outward current, but is blocked by Ba^{2+}, albeit to a lesser extent at positive values (Osterrieder et al. 1982). In addition, in P cells I_K is rather small (<20 pA, Cordeiro et al. 1998) or undetectable (Kenyon and Gibbons 1979). Indeed, in the presence of 4-AP the outward current did not increase with depolarizing steps from V_h −40 mV (Fig. 9).

The increase in peak outward current with steeper ramps in P cells could be due to a larger I_{to} and/or to a lag in I_{K1} block by polyamines which is much slower at positive potentials (Ishihara et al. 1989). In VM cells, with steeper ramps the failure of the ramp peak current to appreciably increase suggests little change in I_{to} whereas the increase in current between ramp peak and I_h indicates a role of I_{K1}.

On repolarization, with respect to VM cells, in P cells the greater fall in current is bound to reflect the much greater I_{to} activated on depolarization, as 4-AP reduced both I_{to} and the decrease in current on repolarization. The finding that on repolarization the decrease in outward current reached a more negative peak in P cells (~−16 mV) than in VM cells (~+7 mV) suggests that on depolarization the less negative reincrease of the outward current in M cells does not entirely depend on being masked by a larger I_{Ca}.

In P cell, I_{to} induces the large phase 1 repolarization of AP, and keeps the plateau at more negative level (Kenyon and Gibbons 1979). In rabbit P cells, 4-AP slowed phase 1 repolarization and shifted the plateau to positive potentials, while having in VM cells a much smaller effect on phase 1 repolarization and no effect on the plateau (Cordeiro et al. 1998).

In P cells, the persistence of the bulge current during the slow ramps and its elimination by 4-AP (which only reduced the sustained current) suggest that in P cells the bulge current is related to the activation of I_{to} whereas the 4-AP resistant increase in outward current toward the ramp peak might reflect a voltage-dependent increase in the sustained current. Another difference is that in VM cells I_{to} markedly decrease with lower V_h whereas in P cells a smaller I_{to} persisted even with V_h −40 (Table 11), consistent with the persistence of the bulge current with V_h −50 mV (Du and Vassalle 1999).

The greater I_{to} in canine P cells has been also found rabbit P cells versus VM cells (Cordeiro et al. 1998). However, in P cells the larger I_{to} and the smaller I_{K1} contributions to the total outward current at the plateau may be important in different situations. For example, an increase rate of discharge (tachycardia) may modify I_{to} (due to its slow recovery; e.g., Cordeiro et al. 1998) more than I_{K1}.

In agreement with the larger I_{to} in P cells, Kv3.4 is more abundant at both the mRNA and protein level in Purkinje fibers than in ventricular myocardium. As the Kv3.4 subunit carries a TEA-sensitive I_{to} outward current, Kv3.4 current may be responsible for the large TEA-sensitive component of I_{to} in canine Purkinje cells (see Schram et al. 2002 for review). Among the differences between I_{to} in P and in VM cells is the different sensitivity to various blockers (e.g., TEA) and a smaller time constant of inactivation in VM cells (Han et al. 2000).

Thus, with respect to the P cells, in VM cells I_{to}: (1) became apparent at more positive potentials during the ramps; (2) did not undergo an enhancement (the "bulge") during depolarizing ramps; (3) was smaller as measured from I_{to} peak either to the end of the step or with respect to I_h; (4) was abolished by 4-AP with a reduced sustained current (as in P cells); (5) had a smaller time constant of inactivation (in agreement with the finding of Han et al. 2000); (6) was associated with smaller slope conductance; (7) during repolarizing ramps, was smaller and had a smaller voltage range; and (8) was inactivated by lower V_h.

General conclusions

The present results indicate substantial differences between P and VM cells that bear on the different functions of P (conduction and pacemaker activity) and VM

cells (contraction). In both tissues, I_{K1} is important for a normal resting potential and its inward rectification is important in more than one way. In P cells, the smaller I_{K1} conductance at the resting potential is essential for pacemaker function in two respects: (1) it keeps the resting potential less negative than E_K and therefore it allows the undershoot to the maximum diastolic potential by the pacemaker current I_{Kdd}; and (2) I_{K1} inward rectification by polyamines contributes to diastolic depolarization caused by time-dependent decay of I_{Kdd} and therefore to the attainment of threshold for I_{Na3}. I_{Na3} initiates I_{NS} and the associated depolarization allows the attainment of I_{Na1} threshold.

Especially in VM cells, I_{K1} inward rectification caused by Mg^{2+} block in the voltage range −40 to 0 mV facilitates the attainment of threshold for Na^+ currents and contributes (see Shimoni et al. 1992) to maintain the plateau. The large and fast I_{Na1} cuts short the no longer needed I_{Na3} and (being large) rapidly depolarizes the membrane and causes the overshoot to positive potentials (fast and large depolarization for rapid conduction). The depolarization induced by I_{Na1} allows the attainment of the thresholds for other currents in an orderly fashion. I_{Na2} (by inactivating slowly in P cells) contributes to their long plateau, thereby preventing the reentry of excitation from myocardium. Once the thresholds for I_{to} and I_{Ca} have been reached, at the end of the upstroke I_{Na1} is rapidly inactivated (thereby preventing a useless Na^+ influx).

The fast activation of I_{to} eliminates the overshoot which is no longer needed for fast conduction. In the meanwhile, I_{Ca} initiates the events leading to contraction and its inactivation balances the inactivating I_{to} at the plateau over a background of I_{K1} inward rectification. In VM cells, I_{Ca} shifted the outward current reincrease by 35 mV and therefore would contribute to the more positive plateau. In P cells, the inwardly rectifying I_{Kdd} becomes activated and whatever slowly decaying I_{Na2} is not inactivated by the end of the plateau becomes deactivated as a function of voltage (Bocchi and Vassalle 2008). During the repolarization, the removal of Mg^{2+} block of the K_1 channels leads to I_{PS} and speeds up phase 3 repolarization, which, in turn, removes the polyamines block. In P cells, I_{Kdd} begins to increase at about I_{PS} peak (~−50 mV, Vassalle et al. 1995) leading to undershoot of resting potential, followed diastolic depolarization.

Among the differences between the two tissues, in P cells the more negative thresholds for the Na^+ currents, the larger I_{Na1} and the larger overshoot contribute to earlier activation and faster conduction. The larger I_{to} contributes to less negative plateau and the slowly inactivating I_{Na2} to the longer AP. The larger sodium influx may involve a higher Na^+-K^+ pump activity, which is the major mechanisms underlying overdrive suppression (Vassalle 1977). Thus, the outward current created by Na^+-K^+ pump activity maintains the diastolic depolarization negative to I_{Na3} threshold, so that P cell spontaneous discharge is suppressed when not needed during sinoatrial rhythm.

In VM cells, the larger resting conductance contributes to set the resting potential near the K^+ equilibrium potential, as a resting potential lower than E_K is needed only for pacemaker activity (see Vassalle 2007, 2013). In VM cells, the smaller I_{Na1} is consistent with the smaller rate of rise of the smaller upstroke (e.g., Baláti et al. 1998), as the conduction path is shorter (from Purkinje network to epicardium). In VM cells, the larger I_{Ca} contributes to stronger contraction (Lin and Vassalle 1978); the smaller I_{to} together with the positive range of the larger I_{Ca} contributes to the more positive plateau. The lack of slowly inactivating I_{Na2} contributes to a shorter AP (which in turn regulates the duration of twitch and of diastole) and the greater I_{K1} and removal of its block during the larger I_{PS} contributes to an earlier and faster phase 3 repolarization.

The definition of these differences is a precondition also for the understanding of deranged function under pathological conditions.

Author Contributions

The experiments were carried out in Dr. Vassalle's lab in the Department of Physiology at SUNY, Downstate Medical Center, Brooklyn, NY. Dr. Vassalle conceived and designed the experiments, participated in part of the experiments, analyzed the data, drew the conclusions and wrote the manuscript. Dr. Bocchi participated in the collection, analysis, and interpretation of the data, their statistical evaluation, and supported various aspects of the writing of the manuscript. All authors approved the final version of the manuscript and qualify for authorship, and all those who qualify for authorship are listed.

Acknowledgments

This work was supported in part by a grant from the National Institutes of Health (HL56092). We thank Dr. Marcello Rota for reading the manuscript and offering helpful criticism.

Conflict of Interest

None declared

References

Abete, P., and M. Vassalle. 1988. Relation among Na^+–K^+ pump, Na^+ activity and force in strophanthidin inotropy in sheep cardiac Purkinje fibres. J. Physiol. 404:275–299.

Baláti, B., A. Varro, and J. G. Papp. 1998. Comparison of the cellular electrophysiological characteristics of canine left ventricular epicardium, M cells, endocardium and Purkinje fibers. Acta Physiol. Scand. 164:181–190.

Berg, D. E., and M. Vassalle. 2000. Oscillatory zones and their role in normal and abnormal sheep Purkinje fiber automaticity. J. Biomed. Sci. 7:364–379.

Bhattacharyya, M. L., and M. Vassalle. 1981. The effect of local anaesthetics on strophanthidin toxicity in canine cardiac Purkinje fibres. J. Physiol. 312:125–142.

Bhattacharyya, M. L., and M. Vassalle. 1982. Effects of tetrodotoxin on electrical and mechanical activity of cardiac Purkinje fibers. J. Electrocardiol. 15:351–360.

Bocchi, L., and M. Vassalle. 2008. Characterization of the slowly inactivating sodium current I_{Na2} in canine cardiac single Purkinje cells. Exp. Physiol. 93:347–361.

Coppini, R., C. Ferrantini, L. Yao, P. Fan, M. Del Lungo, F. Stillitano, et al. 2013. Late sodium current inhibition reverses electro-mechanical dysfunction in human hypertrophic cardiomyopathy. Circulation 127:575–584.

Coraboeuf, E., E. Deroubaix, and A. Coulombe. 1979. Effect of tetrodotoxin on action potentials of the conducting system in the dog heart. Am. J. Physiol. 236:561–567.

Cordeiro, J. M., K. W. Spitzer, and W. R. Giles. 1998. Repolarizing K^+ currents in rabbit heart Purkinje cells. J. Physiol. 508:811–823.

Datyner, N., G. Gintant, and I. S. Cohen. 1985. Microprocessor controlled trituration device for the dissociation of cardiac and other tissues. Pflügers Arch. 403:105–108.

Du, F., and M. Vassalle. 1999. A 4-aminopyridine sensitive current activating during slow ramps in cardiac single Purkinje cells (Abstract). FASEB J. 13:A97.

Dumaine, R., and J. M. Cordeiro. 2007. Comparison of K^+ currents in cardiac Purkinje cells isolated from rabbit and dog. J. Mol. Cell. Cardiol. 42:378–389.

Dun, W., and P. A. Boyden. 2008. The Purkinje cell; 2008 style J. Mol. Cell. Cardiol. 45:617–624.

El-Sherif, N., and G. Turitto. 2003. Torsade de pointes. Curr. Opin. Cardiol. 18:6–13.

Gaborit, N., S. Le Bouter, V. Szuts, A. Varro, D. Escande, S. Nattel, et al. 2007. Regional and tissue specific transcript signatures of ion channel genes in the non-diseased human heart. J. Physiol. 582:675–693.

Gilly, W. F., and C. M. Armstrong. 1984. Threshold channels – a novel type of sodium channel in squid giant axon. Nature 309:448–450.

Han, W., Z. Wang, and S. Nattel. 2000. A comparison of transient outward currents in canine cardiac Purkinje cells and ventricular myocytes. Am. J. Physiol. Heart Circ. Physiol. 279:466–474.

Haufe, V., J. A. Camacho, R. Dumaine, B. Günther, C. Bollensdorff, G. S. von Banchet, et al. 2005a. Expression pattern of neuronal and skeletal muscle voltage-gated Na^+ channels in the developing mouse heart. J. Physiol. 564:683–696.

Haufe, V., J. M. Cordeiro, T. Zimmer, Y. S. Wu, S. Schiccitano, K. Benndorf, et al. 2005b. Contribution of neuronal sodium channels to the cardiac fast sodium current I_{Na} is greater in dog heart Purkinje fibers than in ventricles. Cardiovasc. Res. 65:117–127.

Hirano, Y., and M. Hiraoka. 1986. Changes in K^+ currents induced by Ba^{2+} in guinea pig ventricular muscles. Am. J. Physiol. Heart Circ. Physiol. 251:H24–H33.

Iacono, G., and M. Vassalle. 1990. On the mechanism of the different sensitivity of Purkinje and myocardial fibers to strophanthidin. J. Pharmacol. Exp. Ther. 253:1–12.

Imoto, Y., T. Ehara, and H. Matsuura. 1987. Voltage- and time-dependent block of i_{K1} underlying Ba^{2+} -induced ventricular automaticity. Am. J. Physiol. Heart Circ. Physiol. 252:H325–H333.

Isenberg, G., and U. Klöckner. 1982. Calcium currents of isolated bovine ventricular myocytes are fast and of large amplitude. Pflügers Arch. 395:30–41.

Ishihara, K. 1997. Time-dependent outward currents through the inward rectifier potassium channel IRK1. The role of weak blocking molecules. J. Gen. Physiol. 109:229–243.

Ishihara, K., and T. Ehara. 1998. A repolarization-induced transient increase in the outward current of the inward rectifier K^+ channel in guinea-pig cardiac myocytes. J. Physiol. 510:755–771.

Ishihara, K., T. Mitsuiye, A. Noma, and M. Takano. 1989. The Mg^{2+} block and intrinsic gating underlying inward rectification of the K_1 current in guinea-pig cardiac myocytes. J. Physiol. 419:297–320.

Kenyon, J. L., and W. R. Gibbons. 1979. 4-Aminopyridine and the early outward current of sheep cardiac Purkinje fibers. J. Gen. Physiol. 73:139–157.

Kim, E. M., Y. Choy, and M. Vassalle. 1997. Mechanisms of suppression and initiation of pacemaker activity in guinea pig sino-atrial node superfused in high $[K^+]_o$. J. Mol. Cell. Cardiol. 29:1433–1445.

Lin, C.-I., and M. Vassalle. 1978. Role of sodium in strophanthidin toxicity of Purkinje fibers. Am. J. Physiol. 234:H477–H486.

Liu, B., J. R. McCullough, and M. Vassalle. 1990. On the mechanism of increased potassium conductance by the potassium channel opener BRL 34915 in isolated ventricular myocytes. Drug Dev. Res. 19:409–423.

Lopatin, A. N., and C. G. Nichols. 2001. Inward rectifiers in the heart: an update on I_{K1}. J. Mol. Cell. Cardiol. 33:625–638.

Lopatin, A. N., E. N. Makhina, and C. G. Nichols. 1994. Potassium channel block by cytoplasmic polyamines as the mechanism of intrinsic rectification. Nature 372:366–369.

Matsuda, H., A. Saigusa, and H. Irisawa. 1987. Ohmic conductance through the inwardly rectifying K channel and blocking by internal Mg^{2+}. Nature 325:156–159.

Osterrieder, W., Q. F. Yang, and W. Trautwein. 1982. Effects of barium on the membrane currents in the rabbit S-A node. Pflügers Arch. 394:78–84.

Pu, J., and P. A. Boyden. 1997. Alterations of Na^+ currents in myocytes from epicardial border zone of the infarcted heart. A possible ionic mechanism for reduced excitability and postrepolarization refractoriness. Circ. Res. 81:110–119.

Qu, Y., E. Karnabi, M. Chahine, M. Vassalle, and M. Boutjdir. 2007. Expression of skeletal muscle $Na_V1.4$ Na channel isoform in canine cardiac Purkinje myocytes. Biochem. Biophys. Res. Commun. 355:28–33. Epub

Richmond, J. E., D. E. Featherstone, H. A. Hartmann, and P. C. Ruben. 1998. Slow inactivation in human cardiac sodium channels. Biophys. J. 74:2945–2952.

Rota, M., and M. Vassalle. 2003. Patch-clamp analysis in canine cardiac Purkinje cells of a novel sodium component in the pacemaker range. J. Physiol. 548:147–165.

Schram, G., M. Pourrier, P. Melnyk, and S. Nattel. 2002. Differential distribution of cardiac ion channel expression as a basis for regional specialization in electrical function. Circ. Res. 90:939–950.

Shah, A. K., I. S. Cohen, and N. B. Datyner. 1987. Background K^+ current in isolated canine cardiac Purkinje myocytes. Biophys. J. 52:519–525.

Shimoni, Y., R. B. Clark, and W. R. Giles. 1992. Role of an inwardly rectifying potassium current in rabbit ventricular action potential. J. Physiol. 448:709–727.

Spiegler, P. A., and M. Vassalle. 1995. Role of voltage oscillations in the automaticity of sheep cardiac Purkinje fibers. Can. J. Physiol. Pharmacol. 73:1165–1180.

Tytgat, J., J. Vereecke, and E. Carmeliet. 1990. A combined study of sodium current and T-type calcium current in isolated cardiac cells. Pflügers Arch. 417:142–148.

Valdivia, C. R., W. W. Chu, J. Pu, J. D. Foell, R. A. Haworth, M. R. Wolff, et al. 2005. Increased late sodium current in myocytes from a canine heart failure model and from failing human heart. J. Mol. Cell. Cardiol. 38:475–483.

Valenzuela, F., and M. Vassalle. 1991. Role of the membrane potential on Ba^{2+} -induced automaticity in guinea pig cardiac myocytes. Cardiovasc. Res. 25:421–430.

Vandenberg, C. A. 1987. Inward rectification of a potassium channel in cardiac ventricular cells depends on internal magnesium ions. Proc. Natl Acad. Sci. USA 84:2560–2564.

Vassalle, M. 1965. Cardiac pacemaker potentials at different extra- and intracellular K concentrations. Am. J. Physiol. 208:770–775.

Vassalle, M. 1966. An analysis of cardiac pacemaker potential by means of a "voltage clamp" technique. Am. J. Physiol. 210:1335–1341.

Vassalle, M. 1977. The relationship among cardiac pacemakers: overdrive suppression. Circ. Res. 41:269–277.

Vassalle, M. 1980. The role of the slow inward current in impulse formation. Pp. 127–148 *in* D. P. Zipes, J. C. Bailey, and V. Elharrar, eds. The slow inward current and cardiac arrhythmias. Martinus Nijhoff Publishers, The Hague.

Vassalle, M. 2007. The vicissitudes of the pacemaker current I_{Kdd} of cardiac Purkinje fibers. J. Biomed. Sci. 14:699–716.

Vassalle, M. 2013. Cardiac Purkinje fibers: normal function and its derangements. Pp. 48–86 *in* M. Parveen, ed. Cardiac functioning disorders, challenges and therapies. Japee Medical Publishers, New Delhi & London.

Vassalle, M., and M. Bhattacharyya. 1980. Local anesthetics and the role of sodium in the force development by canine ventricular muscle and Purkinje fibers. Circ. Res. 47:666–674.

Vassalle, M., H. Yu, and I. S. Cohen. 1995. The pacemaker current in cardiac Purkinje myocytes. J. Gen. Physiol. 106:559–578.

Vassalle, M., L. Bocchi, and F. Du. 2007. A slowly inactivating sodium current (I_{Na2}) in the plateau range in canine cardiac Purkinje single cells. Exp. Physiol. 92:161–173.

Vereecke, J., G. Isenberg, and E. Carmeliet. 1980. K efflux through inward rectifying K channels in voltage clamped Purkinje fibers. Pflügers Arch. 384:207–217.

Weidmann, S. 1951. Effect of current flow on the membrane potential of cardiac muscle. J. Physiol. 115:227–236.

Zimmer, T., C. Bollensdorff, V. Haufe, E. Birch-Hirschfeld, and K. Benndorf. 2002. Mouse heart Na^+ channels: primary structure and function of two isoforms and alternatively spliced variants. Am. J. Physiol. Heart Circ. Physiol. 282: H1007–H1017.

Zygmunt, A. C., G. T. Eddlestone, G. P. Thomas, V. V. Nesterenko, and C. Antzelevitch. 2001. Larger late sodium conductance in M cells contributes to electrical heterogeneity in canine ventricle. Am. J. Physiol. 281:H689–H697.